

HOT infrared photodetectors

P. MARTYNIUK and A. ROGALSKI*

Institute of Applied Physics, Military University of Technology,
2 Kaliskiego Str., 00–908 Warsaw, Poland

At present, uncooled thermal detector focal plane arrays are successfully used in staring thermal imagers. However, the performance of thermal detectors is modest, they suffer from slow response and they are not very useful in applications requiring multispectral detection.

Infrared (IR) photon detectors are typically operated at cryogenic temperatures to decrease the noise of the detector arising from various mechanisms associated with the narrow band gap. There are considerable efforts to decrease system cost, size, weight, and power consumption to increase the operating temperature in so-called high-operating-temperature (HOT) detectors. Initial efforts were concentrated on photoconductors and photoelectromagnetic detectors. Next, several ways to achieve HOT detector operation have been elaborated including non-equilibrium detector design with Auger suppression and optical immersion. Recently, new strategies used to achieve HOT detectors include barrier structures such as nBn, material improvement to lower generation-recombination leakage mechanisms, alternate materials such as superlattices and cascade infrared devices. Another method to reduce detector's dark current is reducing volume of detector material via a concept of photon trapping detector.

In this paper, a number of concepts to improve performance of photon detectors operating at near room temperature are presented. Mostly three types of detector materials are considered – HgCdTe and InAsSb ternary alloys, and type-II InAs/GaSb superlattice. Recently, advanced heterojunction photovoltaic detectors have been developed. Novel HOT detector designs, so called interband cascade infrared detectors, have emerged as competitors of HgCdTe photodetectors.

Keywords: HOT detectors, HgCdTe photodetectors, type-II InAs/GaSb superlattice photodetectors, Sb-based III-V photodetectors, photon trapping detectors, cascade infrared detectors.

1. Introduction

Cryogenic cooling of detectors has always been the burden of sensitive infrared (IR) systems. Many efforts have been made to develop imaging IR systems that would not require cryogenic cooling. During the last two decades we have observed a revolutionary emergence of focal plane arrays (FPAs) based on thermal detectors. At present, full TV-compatible arrays are used, but they cannot be expected to replace the high-performance cryogenically cooled arrays without a scientific breakthrough. A response much shorter than that achievable with thermal detectors is required for many applications. Thermal detectors seem to be unsuitable for the IR thermal imaging systems, which are moving toward faster frame rates and multispectral operation. A response time much shorter than that achievable with thermal detectors is required for many non-imaging applications. Photon detectors (photodetectors) make it possible to achieve both high sensitivity and fast response. Recent considerations of the fundamental photodetector mechanisms suggest that, in principle, near-perfect detection can be achieved in the mid wavelength IR (MWIR) and long wavelength

IR (LWIR) ranges without the need for cryogenic cooling [1–3].

Progress in IR photodetector technology is mainly connected with semiconductor IR detectors. The most important are photodetectors fabricated with narrow-gap semiconductors, especially with HgCdTe. To obtain high performance detectors, temperatures much lower than 300 K are required (typically 80–200 K). Cooling requirements significantly increase price and size of IR systems, therefore, one of the main research goals is an increase in working temperature of photodetectors.

A number of concepts to improve performance of the near room temperature IR photodetectors have been proposed. Apart from photoconductive detectors and photodiodes [4], three other types of IR photodetectors can operate at near room temperature; photoelectromagnetic (or PEM) detectors, magnetoconcentration detectors and Dember effect detectors [1,5]. While significant improvements have been obtained by suppression of Auger thermal generation in excluded photoconductors [6], extracted photodiodes [6–8], and magnetoconcentration effect detectors [9,10], these non-equilibrium devices require significant bias currents and exhibit excessive low frequency 1/f noise that extends up to MHz range. A new strategies used to achieve HOT detectors

* e-mail: rogan@wat.edu.pl

include barrier structures such as nBn, material improvement to lower generation-recombination leakage mechanisms, alternate materials such as superlattices and cascade infrared devices.

Here we review the progress in development of uncooled IR infrared photon detectors called HOT (high-operating-temperature) photodetectors. The paper presents approaches, materials, and devices that eliminate the cooling requirements of IR photodetectors operating in the middle- (MW) and long-wavelength (LW) ranges of the IR spectrum. An approach to reduce photodetector cooling requirements based on non-equilibrium mode of operation [11] and proposed by British workers is omitted in our considerations. Progress in developments of HgCdTe HOT photodetectors described in details in recently published papers (see, e.g., Refs. 1–3) is presented here shortly. Instead in this paper we concentrate on novel HOT devices developed in the last decade, mainly on nBn and cascade infrared devices.

2. Fundamental performance limits of HOT photodetectors

In general, the detector can be considered as a slab of homogeneous semiconductor with actual “electrical” area, A_e , and thickness t (see Fig. 1). Usually, the optical and electrical areas of the device are the same or similar. However, the use of some kind of optical concentrator can increase the A_o/A_e ratio by a large factor.

The current responsivity of the photodetector is determined by the quantum efficiency, η , and by the photoelectric gain, g . The quantum efficiency is defined here as the number of electron-hole pairs generated per incident photon in a detector, instead the photoelectric gain is the number of carriers passing contacts per one generated pair in a detector. This value shows how well the generated charge carriers are used to generate current response of a photodetector. Both values are assumed here as constant over the volume of the device.

The spectral current responsivity is equal to

$$R_i = \frac{\lambda\eta}{hc} qg, \quad (1)$$

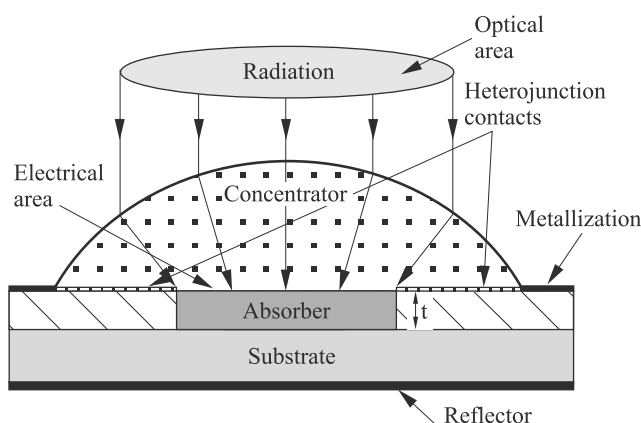


Fig. 1. Model of a photodetector.

where λ is the wavelength, h is the Planck's constant, c is the velocity of light, q is the electron charge, and g is the photoelectric current gain.

The performance of infrared photodetectors is limited by statistical nature of generation and recombination of charge carriers in the semiconductor. The current that flows through the contacts of the detector is noisy due to the statistical nature of the generation and recombination processes – fluctuation of optical generation, thermal generation, and radiative and nonradiative recombination rates. Assuming that the current gain for the photocurrent and the noise current are the same, the noise current is [2]

$$I_n^2 = 2q^2 g^2 (G_{op} + G_{th} + R)\Delta f, \quad (2)$$

where G_{op} is the optical generation rate, G_{th} is the thermal generation rate, R is the resulting recombination rate, and Δf is the frequency band.

Optical generation noise is photon noise due to fluctuation of the incident flux. The optical generation of the charge carriers may result from three different sources: signal radiation generation, background radiation generation, and thermal self-radiation of the detector itself at a finite temperature. Usually, the noise due to optical signal flux is small compared to the contributions from background radiation or thermal generation-recombination processes. An exception is heterodyne detection, when the noise due to the powerful local oscillator radiation may dominate.

Background radiation is frequently the main source of noise in a detector. Assuming no contribution due to recombination,

$$I_n^2 = 2\Phi_B A_o \eta q^2 g^2 \Delta f, \quad (3)$$

where Φ_B is the background photon flux density. Therefore,

$$D_{BLIP}^* = \frac{\lambda}{hc} \left(\frac{\eta}{\Phi_B} \right)^{1/2}. \quad (4)$$

Once background-limited performance is reached, quantum efficiency, η , is the only detector parameter that can influence a detector's performance.

Figure 2 shows the peak spectral of a photon counter vs. the cut-off wavelength plot calculated for 300 K background radiation and hemispherical field of view (FOV) ($\theta = 90$ deg). The minimum D_{BLIP}^* (300 K) occurs at 14 μm and is equal to $4.6 \times 10^{10} \text{ cmHz}^{1/2}/\text{W}$. For some photodetectors that operate at near equilibrium conditions, such as non-sweep-out photoconductors, the recombination rate is equal to the generation rate. For these detectors the contribution of recombination to the noise will reduce D_{BLIP}^* by a factor of $2^{1/2}$. Note that D_{BLIP}^* does not depend on area and the A_o/A_e ratio. As a consequence, the background limited performance cannot be improved by making A_o/A_e large.

Infrared photodetectors operating at near room temperature are generally limited by thermal generation and recombination mechanisms rather than by photon noise. For effective absorption of IR radiation in a semiconductor, we must

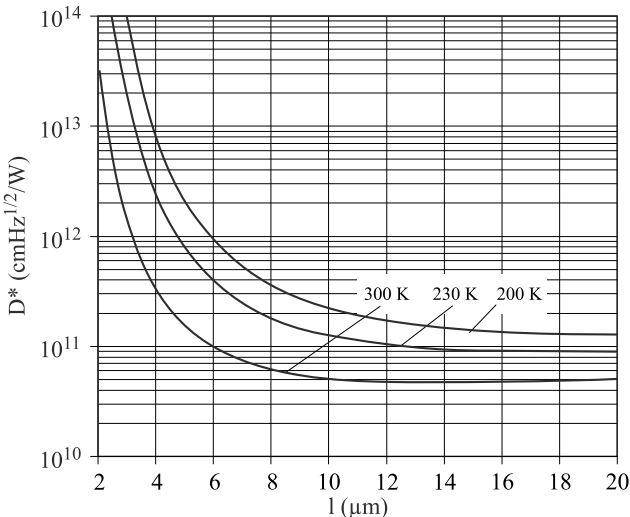


Fig. 2. Calculated peak spectral detectivities of a photon counter limited by the hemispherical FOV background radiation as a function of the peak wavelength and temperature (after Ref. 2).

use material with a low energy of optical transitions compared to the energy of photons to be detected – for example, semiconductors with a narrower band gap. A direct consequence of this fact is that at near room temperatures, the thermal energy of charge carriers, kT , becomes comparable to the transition energy. This enables thermal transitions, making the thermal generation rate very high. As a result, the long-wavelength detector is very noisy when operated at near room temperature.

For uniform volume generation and recombination rates G and R (in $\text{m}^{-6}\text{s}^{-1}$), the noise current is

$$I_n^2 = 2(G+R)A_e t \Delta f q^2 g^2, \quad (5)$$

therefore,

$$D^* = \frac{\lambda}{2^{1/2} hc(G+R)^{1/2}} \left(\frac{A_o}{A_e} \right)^{1/2} \frac{\eta}{t^{1/2}}. \quad (6)$$

At equilibrium, the generation and recombination rates are equal. In this case

$$D^* = \frac{\lambda \eta}{2hc(Gt)^{1/2}} \left(\frac{A_o}{A_e} \right)^{1/2}. \quad (7)$$

For a given wavelength and operating temperature, the highest performance can be obtained by maximizing $\eta/[(G+R)t]^{1/2}$. This is the condition for the highest ratio of the quantum efficiency to the square root of the sum of the sheet thermal generation and recombination rates. This means that high quantum efficiency must be obtained with a thin device.

A possible way to improve the performance of IR detectors is to reduce the physical volume of the semiconductor, thus reducing the amount of thermal generation. This must be done without decrease in quantum efficiency, optical area, and field of view (FOV) of the detector. These issues

are discussed, e.g., in Refs. 2 and 3 and in Sect. 5 of this paper devoted to photon trapping detectors.

The detectivity of an optimized infrared photodetector is limited by thermal processes in the active region of the device. It can be expressed as [12,13]

$$D^* = 0.31 \frac{\lambda}{hc} k \left(\frac{\alpha}{G} \right)^{1/2}, \quad (8)$$

where $1 \leq k \leq 2$, and k is dependent on the contribution of recombination and backside reflection.

The ratio of the absorption coefficient to the thermal generation rate, α/G , is the fundamental figure of merit of any material intended for infrared photodetectors. Analysis shows, that the narrow gap semiconductors are more suitable for high temperature photodetectors in comparison to competing technologies such as extrinsic devices, Schottky barrier, QWIP (quantum well IR photodetector) and QDIP (quantum dot IR photodetector) devices. The main reason for high performance of intrinsic photodetectors is high density of states in the valence and conduction bands, which results in strong absorption of infrared radiation.

It is interesting to consider the performance requirements of near room temperature photodetectors for thermal cameras. Thermal resolution of infrared thermal systems is usually characterized by the noise equivalent temperature difference ($NETD$). It can be shown, that [4]

$$NETD = \frac{4F^2 \Delta f^{1/2}}{A_d^{1/2} t_{op}} \left[\int_{\lambda_a}^{\lambda_b} \frac{dM}{dT} D^*(\lambda) d\lambda \right]^{-1}, \quad (9)$$

where F is the optics f-number, Δf is the frequency band, A_d is the detector area, t_{op} is the optics transmission, M is the spectral emittance of the blackbody described by the Planck's law.

As Eq. (9) shows, the thermal resolution improves with an increase in detector area. Increasing detector area results in reduced spatial resolution, however. Hence, a reasonable compromise between the requirement of high thermal and spatial resolution is necessary. Improvement of thermal resolution without spatial resolution worsening may be achieved by:

- increase of detector area combined with corresponding increase of focal length and the objective aperture;
- improved detector performance;
- increased number of detectors.

Increase of aperture is undesirable because it increases sizes, mass and price of an IR system. It is more proper to use a detector with higher detectivity. Another possibility is the application of multi-elemental sensor, what reduces each element bandwidth proportionally to the number of elements for the same frame rate and other parameters.

Figure 3 shows the dependence of detectivity on cut-off wavelength for a photon counter detector thermal imager with a resolution of 0.1 K. Detectivities of 1.9×10^8 $\text{cmHz}^{1/2}/\text{W}$, 2.3×10^8 $\text{cmHz}^{1/2}/\text{W}$, and 2×10^9 $\text{cmHz}^{1/2}/\text{W}$ are necessary to obtain $NETD = 0.1$ K for $10 \mu\text{m}$, $9 \mu\text{m}$, and

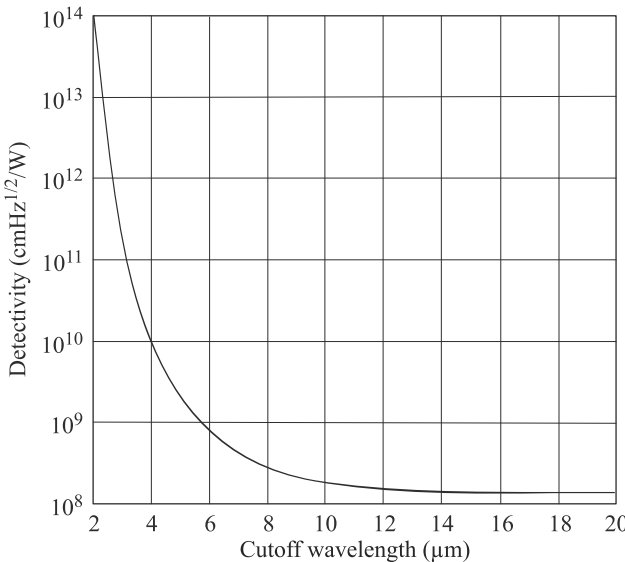


Fig. 3. Detectivity needed to obtain $NEDT = 0.1 \text{ K}$ in a photon counter detector thermal imager as a function of cut-off wavelength (after Ref. 1).

5 μm cut-off wavelength photon counter detectors, respectively. The above estimations indicate that the ultimate performance of the uncooled photodetectors is not sufficient to achieve the required 0.1 K thermal resolution. The thermal resolution below 0.1 K is achieved for staring thermal imagers containing thermal detector focal plane arrays.

3. Infrared HOT detectors

3.1. HgCdTe detectors

The HgCdTe ternary alloy is a close to ideal infrared detector material system. Its unique position is dependent on three key features:

- composition-dependent tailor able energy band gap over the entire 1–30- μm range,
- large optical coefficients that enable high quantum efficiency, and
- favourable inherent recombination mechanisms that lead to long carrier lifetime and high operating temperature.

These properties are a direct consequence of the energy band structure of this zinc-blende semiconductor. Moreover, additional specific advantages of HgCdTe are the ability to obtain both low and high carrier concentrations, high mobility of electrons, and low dielectric constant. The extremely small change of lattice constant with composition makes it possible to grow high quality layered and graded gap structures. As a result, HgCdTe can be used for detectors operated in various modes, photoconductor, photodiode or metal-insulator-semiconductor (MIS) detector.

In the case of HgCdTe HOT devices, a moderate p-type doping of the absorber detector region is widely used for some suppression of the Auger mechanisms. More efficient suppression can be obtained with non-equilibrium depletion of the semiconductor. However, the non-equilibrium mode

devices suffer from a high level of flicker noise that make them useless for most of practical applications that require detection of IR radiation in the low and moderate frequency range. An example is thermal imaging.

The most popular HgCdTe HOT photodetectors are photoconductors and photodiodes. Apart from these devices, three other junctionless niche devices have been used for uncooled IR photodetectors [2,3,5]: PEM detectors, magnetoconcentration detectors, and Dember effect detectors. They are still manufactured by Vigo Systems [14] and are used for some applications, including very fast uncooled detection of LWIR radiation. The state-of-the-art of HgCdTe HOT detectors has been recently reviewed by Józef Piotrowski and his son – Adam Piotrowski [3]. Here we shortly describe only the most important recent achievements in fabrication of Vigo's detectors [15].

The performance of conventional p-n junction LWIR HgCdTe photovoltaic detectors operating at near room temperature is very poor due to a low quantum efficiency (low diffusion length and weak absorption of radiation) and a low dynamic resistance. Only charge carriers that are photo-generated at distance shorter than the diffusion length from junction can be collected. The absorption depth of long wavelength IR radiation ($\lambda > 5 \mu\text{m}$) is longer than the diffusion length. Therefore, only a limited fraction of the photo-generated charge contributes to the quantum efficiency. Consider an example of an uncooled 10.6- μm photodiode. Calculations show that the ambipolar diffusion length is less than 2 μm while the absorption depth is $\approx 13 \mu\text{m}$. This reduces the quantum efficiency to $\approx 15\%$ for a single pass of radiation through the detector.

The Polish scientific and fabrication possibilities connected with development of new generation of HOT HgCdTe photodetectors considerably increased after creation from the ground, in March 2003, a common Vigo-MUT (Military University of Technology) MOCVD laboratory and installation of Aixtron Aix-200 II-VI system dedicated to HgCdTe ternary alloys.

Vigo Systems have developed a monolithic 3-dimensional HgCdTe photodetector concept that integrates optical (concentration of signal radiation, multipass of radiation),



Fig. 4. Monolithically integrated TE-cooled HgCdTe Vigo's detector (with GaAs-microlens) just before final packaging (courtesy Vigo Systems).

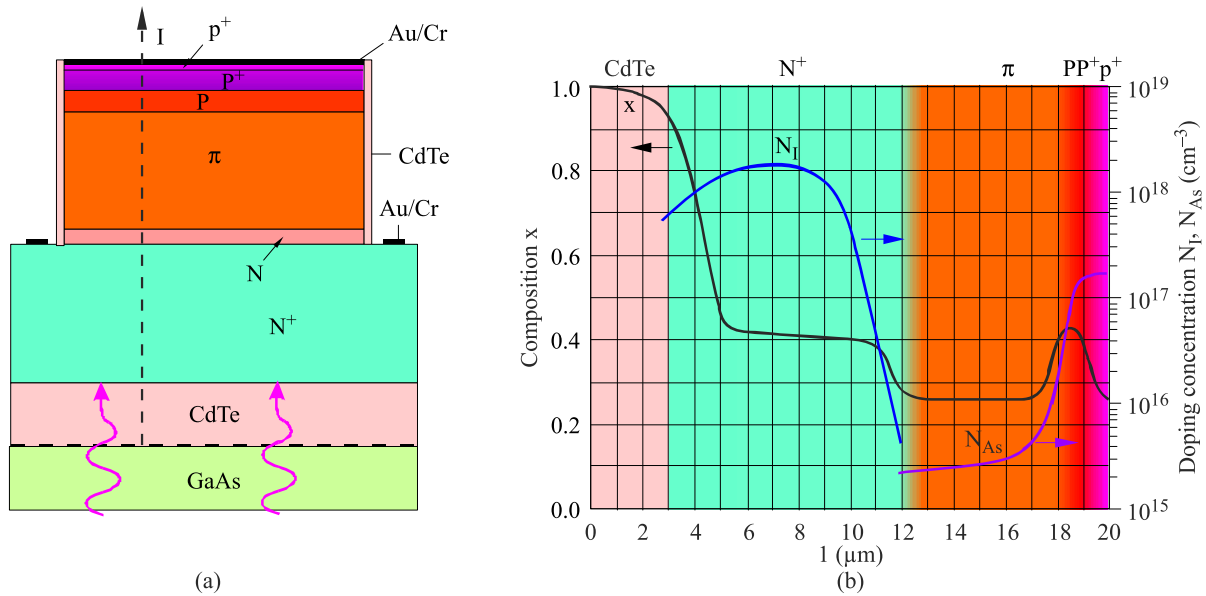


Fig. 5. HgCdTe heterostructure photodiode: schematic structure (a) and composition and doping profiles (b) (courtesy Vigo Systems).

detection (absorption, charge collection), and electronic (photoelectric gain) functions in a monolithic chip – see Figs. 1 and 4. Such devices achieve good parameters without cryogenic cooling what gives them a competitive advantage over detectors available on the market, especially in such applications as gas analyze systems and infrared spectroscopy.

Figure 5(a) shows the PIN-type HgCdTe photodiode heterostructure for near room temperature operation. The detector heterostructure region consists up to 7 layers (with different compositions and doping; the details of detector design are described, e.g., in Refs. 2, 3, 16 and 17). In order to realize the potential of improving device performance, suitable dopants have to be selected. Currently, the most commonly used dopants for MOCVD growth are arsenic (As) as the p-type dopant and iodine (I) as the n-type dopant. Figure 5(b) presents the composition and doping profiles of the heterostructure with active π -region. The heavily doped wide gap N⁺ and P⁺ regions play a role in the majority and minority carrier contacts that do not introduce minority carriers to the absorber and protect the device against dark current generation at surfaces. In addition, the heavy doping makes it possible to achieve low resistance contacts. Less doped wide gap P and N layers are placed between absorber

and the heavy doped regions to reduce interface thermal generation and tunnel currents.

The resistance of the p-n junction is very low due to a high thermal generation. In materials with a high electron to hole mobility ratio, the resistance is additionally reduced by ambipolar effects. As a result, the preamplifier noise and noise of parasitic resistances may exceed the thermal generation-recombination noise. As a result, the performance of devices is poor, so they are not usable for practical applications. This can be overcome with development of multiple heterojunction photovoltaic devices in which short elements were connected in series. An example is a device with junction's planes perpendicular to the substrate [Fig. 6(a)]. The multi-heterojunction device consisted of a structure based on backside illuminated n⁺-p-P photodiodes. This device was the first commercially available uncooled and unbiased long wavelength photovoltaic detector introduced in 1995. Such devices are characterized by large voltage responsivity, fast response time, but they suffer from non-uniform response across the active area and dependence of response on polarization of incident radiation.

More promising are the stacked photovoltaic cells monolithically connected in series shown in Fig. 6(b). They are capable of achieving both good quantum efficiency and

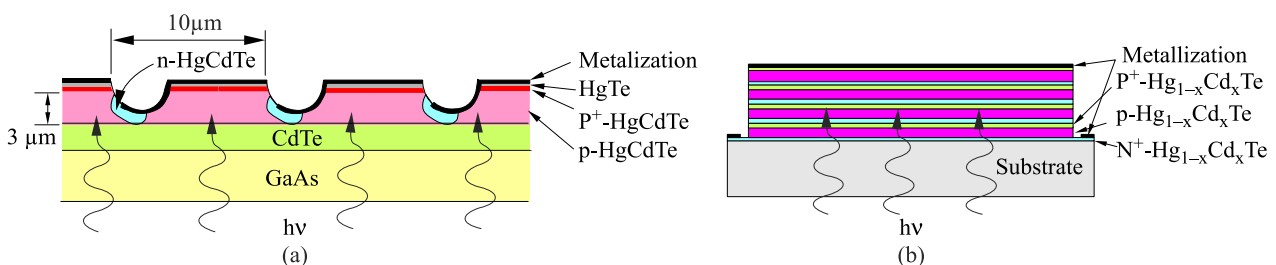


Fig. 6. Backside illuminated multiple HgCdTe heterojunction devices: (a) junction's planes perpendicular to the surface, and (b) 4-cells stacked multiple detector (after Ref. 2).

a large differential resistance. Each cell is composed of p-type doped narrow gap absorber and heavily doped N⁺ and P⁺ heterojunction contacts. The incoming radiation is absorbed only in absorber regions, while the heterojunction contacts collect the photogenerated charge carriers. Such devices are capable of achieving high quantum efficiency, large differential resistance and fast response. The practical problem is the shortage of adjacent N⁺ and P⁺ regions. This can be achieved employing tunnel currents at the N⁺ and P⁺ interface.

At present, VIGO System offers photovoltaic devices optimized at any wavelength in the LWIR, MWIR, and SWIR range of infrared spectrum [14]. The longest usable wavelength is 11 μm, 13 and 15 μm for uncooled, 2- and 3-stage Peltier coolers, respectively.

Figure 7 shows the performance of the HgCdTe devices. Without optical immersion MWIR photovoltaic detectors are sub-BLIP devices with performance close to the generation-recombination limit, but well-designed optically immersed devices approach BLIP limit when thermoelectrically cooled with 2-stage Peltier coolers. Situation is less favourable for > 8-μm LWIR photovoltaic detectors; they show detectivities below the BLIP limit by an order of magnitude. Typically, the devices are used at zero bias. The attempts to use Auger suppressed non-equilibrium devices were not successful due to large 1/f noise extending to ≈100 MHz in extracted photodiode.

The HOT devices are characterized by a very fast response. The uncooled ≈10 μm photodetectors show ≈1 ns or less response time. The RC time constant of photovoltaic devices can be shorten by the use of optical immersion to reduce physical area of devices [2]. The series resistance was minimized to ≈1 Ω using heavily doped N⁺ for base regions of the mesa structures and improved anode contact.

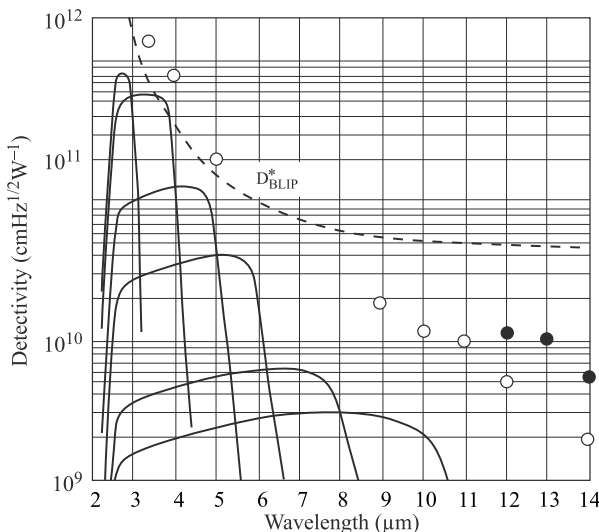


Fig. 7. Typical spectral detectivity of HgCdTe detectors with 2-stage TE coolers (solid lines). The best experimental data (white dots) are measured for detectors with field of view (FOV) equal 36 degrees. BLIP detectivity is calculated for FOV = 2π . Black dots are measured for detectors with 4-stage TE coolers.

3.2. Sb-based III-V photodetectors

As an alternative to the current market dominant HgCdTe, several III-V semiconductor systems such as InAs_{1-x}Sb_x (InAsSb) [18] and InAs/GaSb type-II superlattices (T2SLs) have been proposed [19].

For a long time, the PEM effect has been used mostly for InSb room temperature detectors in the middle- and longer wavelength IR band [20]. However, the uncooled InSb devices with a cut-off wavelength at ≈7 μm exhibit no response in the 8–14-μm atmospheric window and relatively modest performance in the 3–5-μm window.

More recently, the InSb photodiodes grown heteroepitaxially on Si and GaAs substrates by MBE have been also reported [21]. Kuze *et al.* [22,23] have developed a novel microchip-sized InSb photodiode sensor, on semi-insulating GaAs(100) substrate. The sensor consists of 910 photodiodes connected in series (see Fig. 8). Each photodiode consists of MBE grown 1-μm-thick n⁺-InSb layer, followed by a 2-μm-thick π-InSb absorber layer. To reduce the diffusion of photo-excited electrons, a 20-nm thick p⁺-Al_{0.17}In_{0.83}Sb barrier layer was grown on the π-InSb layer. Finally, a 0.5-μm-thick π-InSb layer was grown as the top contact. As the n- and p-type dopants Sn and Zn were used, respectively, with the concentrations of 7×10^{18} cm⁻³ for the n⁺-layer, 6×10^{16} cm⁻³ for the π-layer, and 2×10^{18} cm⁻³ for the p⁺-layer. To insulate mesa structures, a 300-nm thick plasma CVD passivation Si₃N₄ layer was deposited. Finally, after Ti/Au lift-off metallization, a 300-nm thick SiO₂ passivation also grown by plasma CVD was made. The length of single InSb photodiode was 20 μm. The final external dimensions of photovoltaic infrared sensor were 1.9×2.7×0.4 mm³ [see Fig. 8(c)].

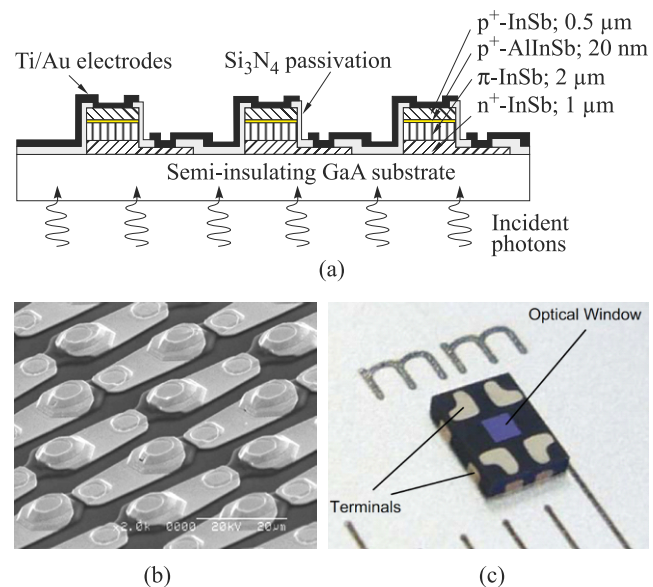


Fig. 8. InSb photovoltaic infrared sensor: (a) schematic structure of multiple photodiodes connected in series, (b) SEM photograph, and (c) picture of a dual flat non-leaded packaged InSb sensor (after Refs. 22 and 23).

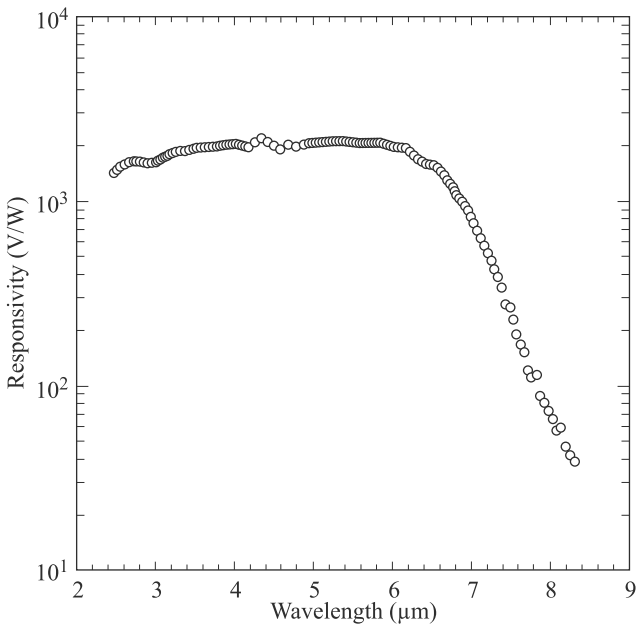


Fig. 9. Spectral response of InSb photovoltaic infrared sensor (700 photodiodes connected in series) at room temperature (after Ref. 22).

InSb photovoltaic sensor can be used both in non-contact thermometry, as well as human body detection. Its peak responsivity about 1.9 kV/W is between 5 and 6 μm ; the cut-off wavelength $\lambda_c = 6.8 \mu\text{m}$ (Fig. 9). The sensitivity and the noise equivalent difference temperature were estimated to be 127 $\mu\text{V/K}$ and 1 mK/Hz $^{1/2}$, respectively [23].

Earlier data suggest that InAs $_{1-x}$ Sb $_x$ can exhibit a cut-off wavelength up to 12.5 μm at 300 K (the minimum of energy gap appears at composition $x = 0.65$) [24]. However, some

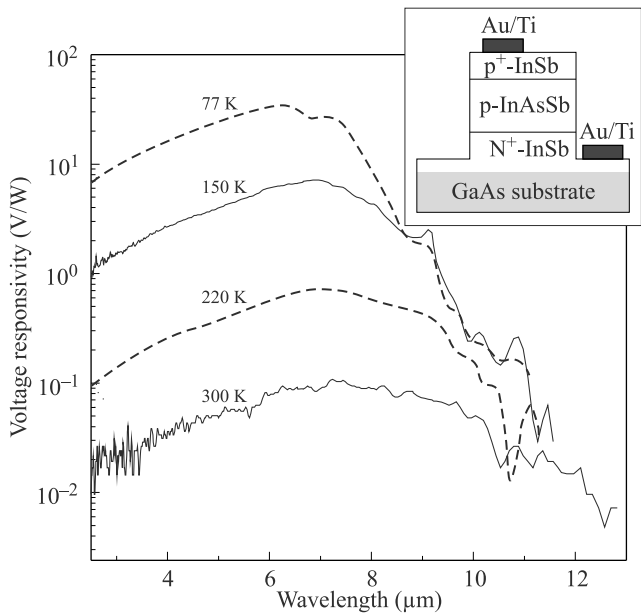


Fig. 10. Spectral voltage responsivity of p^+ -InSb/ p -InAs $_{0.15}$ Sb $_{0.85}$ / n^+ -InSb heterojunction photodiode. Schematic of a photodiode structure is shown in the insert (after Ref. 18).

experimental results demonstrated that the cut-off wavelength of epitaxial layers can be longer than 12.5 μm , thus covering the entire 8–14 μm at near room temperature. This may be due to a structural ordering.

InAsSb photoconductive detectors were fabricated on p -InAsSb/ p -InSb heterostructures. A room temperature photoresponse up to $\approx 14 \mu\text{m}$ has been obtained at 300 K [18]. From the voltage dependent responsivity measurement, an effective lifetime of about 0.14 ns has been obtained. The estimated detectivity at $\lambda = 10.6 \mu\text{m}$ is limited by Johnson noise at the level of about $3 \times 10^7 \text{ cmHz}^{1/2}/\text{W}$ at 300 K.

Photovoltaic devices consist of a double heterojunction of p^+ -InSb/ π -InAs $_{1-x}$ Sb $_x$ / n^+ -InSb on (001)GaAs (see Fig. 10). In spite of the large lattice mismatch between the InAsSb and GaAs, InAsSb detectors have exhibited good characteristics and showed their feasibility for the near room temperature LWIR photodetectors. The photodiode optimized for $\lambda = 10.6 \mu\text{m}$ was characterized by the detectivity of $\approx 1.5 \times 10^8 \text{ cmHz}^{1/2}/\text{W}$.

Type-II superlattices have been proposed as another alternative for uncooled infrared photodetectors in the LWIR range [19]. In comparison to HgCdTe, the higher effective mass of electrons and holes and the slower Auger recombination rate lead to lower dark current and higher operating temperature in type-II superlattices. Unlike type-I superlattices, one can modify the energy of the conduction and valence minibands of a type-II superlattice with a high degree of freedom.

InAs/GaSb T2SLs were grown by MBE on semi-insulating (001)GaAs substrates. Photoconductive detectors fabricated from the superlattices showed 80% cut-off at about 12 μm . The responsivity of the device (see Fig. 11) is about 2 mA/W with a 1 V bias (electrical field 5 V/cm) and the maximum measured detectivity of the device is $1.3 \times 10^8 \text{ cmHz}^{1/2}/\text{W}$ (without any immersion lens and antireflector coating) at 11 μm at room temperature. The detector shows very weak temperature sensitivity. The carrier lifetime, $\tau = 6 \text{ ns}$, is an order of magnitude longer than the carrier life-

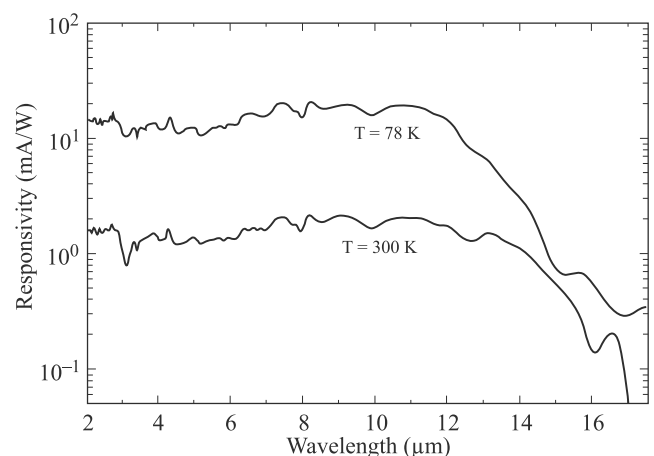


Fig. 11. Responsivity spectra of the device at 78 and 300 K with an in-plane electrical field of 5 V/cm (after Ref. 19).

time in HgCdTe with similar bandgap and carrier concentration. This evidences suppression of Auger recombination in this material system.

4. HgCdTe HOT focal plane arrays

Activity of Vigo Systems concerns on production of single and linear array HgCdTe HOT photodetectors with optical immersion which are exported now to many countries in the world. In the case of large IR focal plane arrays (FPAs) raising of detector's temperature operation has benefits in terms of reduced cooler power and increased life and enables an overall reduction in size, weight, and power (SWaP) for handheld applications. Low-power, large-format, small-pixel IR FPAs with large dynamic, on-chip digital image processing (for SWaP-efficient sensor designs) and high-speed readout (for large-area coverage) are now possible. At present, an extraordinary HOT HgCdTe detector technology, which can perform at significantly elevated temperatures to minimize these trade-offs are developed.

Advances in HgCdTe MOCVD growth technology at Selex Galileo have allowed increased operating temperatures of MWIR FPAs [25,26]. HOT detector structures are as-grown N⁺-p mesa heterostructure shown in Fig. 12(a). A thicker common layer enables deeper etching and reduced

absorber layer volume in individual pixels to suppress dark current without loss of photocurrent. The mesa array geometry also permits a degree of optical concentration into a reduced area p-n junction towards the mesa top, with possible improvements in dark current. Figure 12(b) illustrates the mesa structures of focal plane array.

A key factor in determining the dark current is the role of recombination centres in the generation-recombination process. DeWames and Pellegrino [27] presented a carrier recombination model that explains the measured dark current density as a function of temperatures for N⁺-p(As) Selex devices grown by MOVPE on GaAs. They proposed a donor-like recombination centre with very fast electron capture and slower hole capture. Their fit to the experimental data was consistent with a trap energy 86 meV below the conduction band edge and the hole lifetime of 550 μs. Interestingly, the band-to-band recombination mechanisms (radiative and Auger processes) are not limiting the observed dark current density, even in the region of higher temperature operation where these processes are dominant. Possible explanations include photon recycling or suppression of band to band transitions by very fast capture of excess minority carriers (electrons) by the “empty” set of donor flaws. So, the deliberate introduction of recombination centres has emerged as a new technique in HOT detector engineering.

This new processing of MWIR HgCdTe photodiode arrays grown by MOCVD was adapted by Selex to achieve high performance at high operating temperatures. The Hawk 16-μm pitch full TV detector (640×512 pixels) with 5-μm cut-off wavelength and f/4 aperture demonstrates good quality image at temperatures of 160–190 K. Although the acceptable 210-K image is slightly grainier than the 160-K image, the 210-K image is very useable (see Fig. 13).

For standard production arrays (results from the 2011) the median noise equivalent difference temperature (*NEDT*) remains constant up to 150–160 K and doubles by 185 K (see Fig. 14). The performance limitations are

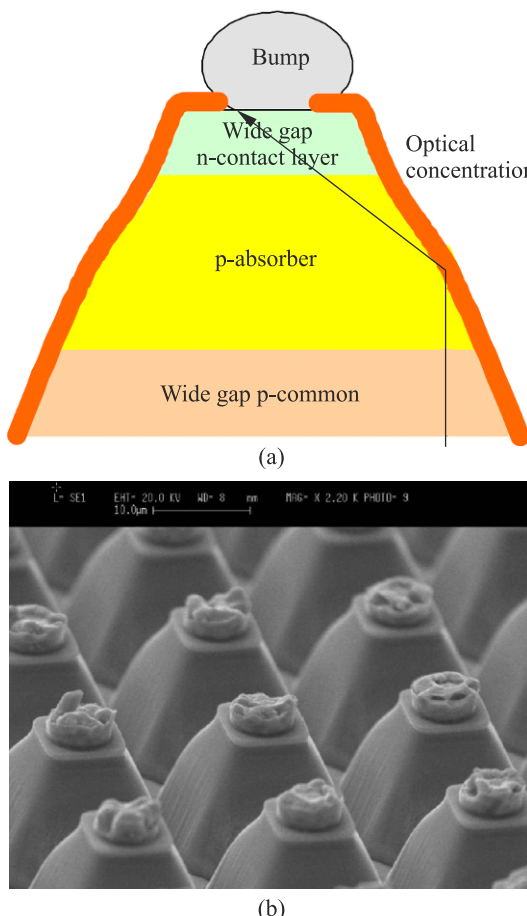


Fig. 12. HOT MWIR N⁺-p HgCdTe photodiode: (a) single detector structure and (b) focal plane array (after Ref. 25).



Fig. 13. Hawk image at 210K operating temperature (after Ref. 26).

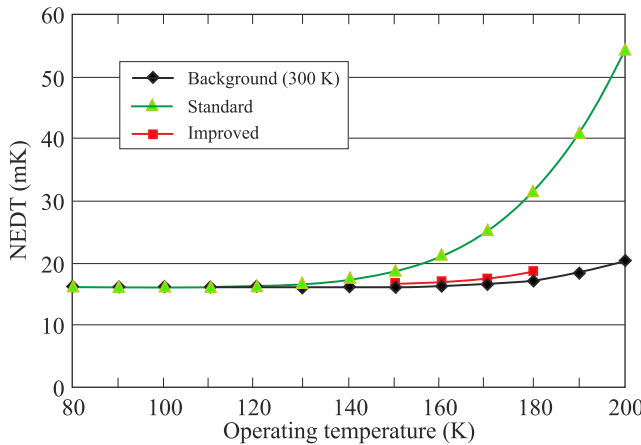


Fig. 14. Predicted NETD performance as a function of operating temperature (after Ref. 25).

believed to originate from array processing technology where dark currents start to impact performance above 150 K and noticeable but not prohibitive rises in NETD are observed above 160 K. The new results clearly predict an improvement in HOT performance over the standard production arrays and significantly extend the useful range of operating temperatures. The near-background limited performance achieved at 150 K by the standard process has been raised around 30 K to 180 K with the expectation of background-dominated performance to well above 200 K (see Fig. 14).

Increasing the operating temperature of detector reduces the cooling load allowing more compact engines with higher efficiency. For an operating temperature of 150 K, the cool-down time and steady state power dissipation in the standard Hawk integrated dewar cooler assembly (IDCA) are reduced by around 40% and 55%, respectively compared with 80 K operation (see Fig. 15). To achieve near BLIP performance at temperatures above 150 K, the previously optimised engine cooled configuration consumed 1–2 W in steady state. At present, similar performance at temperatures in the range of 200–220 K introduces the opportunity for thermoelectrically cooled operation.

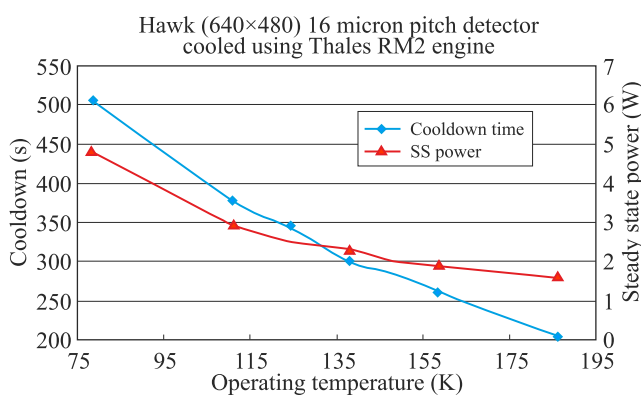


Fig. 15. HAWK IDCA performance in room temperature ambient (power excludes cooler control electronics losses) (after Ref. 26).

5. Photon trapping detectors

As indicates Eq. (7), the performance of infrared detector can be improved by reducing volume of active detector's region. In this part of paper we focus our considerations on reducing detector material via a concept of photon trapping detector. Reducing of the dark current should be achieved without degrading quantum efficiency. Figure 16 shows the effect of volume reduction on quantum efficiency and NETD [28,29] using a simple first-order model consisting of the Bruggeman effective-medium [30] combining HgCdTe with a composition $x \approx 0.3$ with void material. The fill factor is calculated as the volume of material remaining divided by the volume of the unit cell. As it is possible to expect, the effect of volume reduction is to improve performance until a critical point when the volume reduction removes so much material that the decreased collection, and hence response, is more than the decrease in noise, and hence performance degrades. The modelled trends are observed in measured devices.

Since absorption coefficient is a strong function of the wavelength, the wavelength range in which an appreciable photocurrent can be generated is limited for a given detector material. So, broadband absorption is usually inadequate due to quantum efficiency roll-off. To improve charge collection of photons with varying wavelengths application, the photonic crystals to IR detectors are applied [31]. Krishna *et al.* [32] have reported quantum efficiency improvement from 7% to 93% for reverse biased DWELL detector.

Photon trapping detectors have been demonstrated independently in II–VI and III–V based epitaxial materials [31–34]. Sub-wavelength size semiconductor pillar arrays within a single detector are designed and structured as an ensemble of 3D photonic structure units using either a top-down or bottom-up process scheme to significantly increase absorption and quantum efficiency. The sub-element architecture can be of different shapes such as pyramidal, sinusoidal or rectangular [33]. For example, Figure 17(a) shows the photon trap structures with pillars and holes of varying volume fill factors. These samples were fabricated

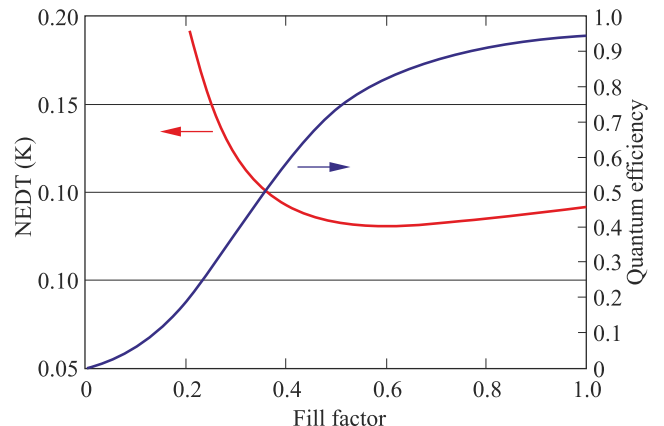


Fig. 16. Effect of volume reduction on quantum efficiency and noise equivalent temperature difference (after Ref. 29).

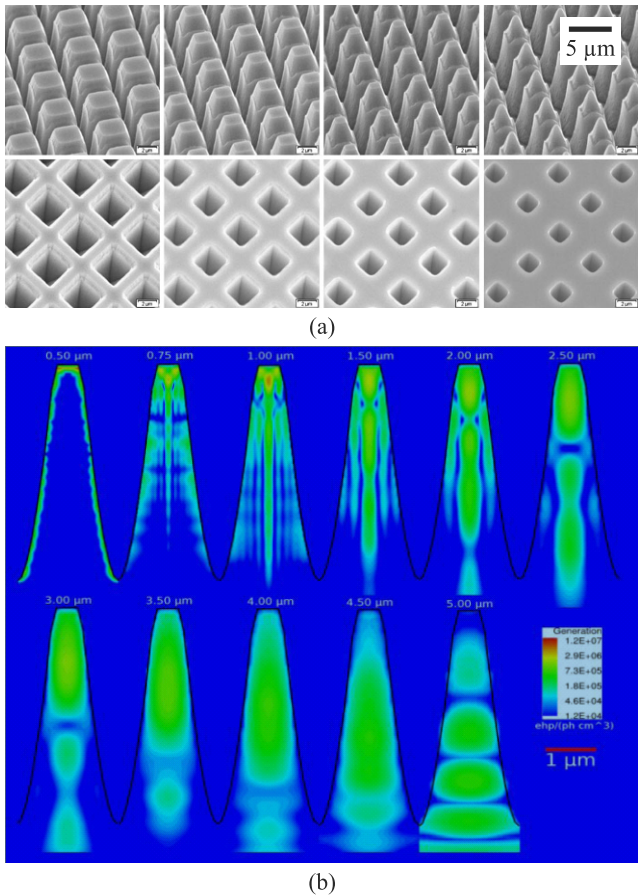


Fig. 17. Photon trap HgCdTe microstructures: (a) examples of test photonic crystal fields with varying fill factor for FTIR demonstration (after Ref. 28), and (b) electromagnetic simulation of pillared material (after Ref. 33).

from HgCdTe layers on Si grown by MBE with cut-off of 5 μm at 300 K. Finite-difference time-domain (FDTD) simulation of pillar structures indicates resonance between them [see Fig. 17(b)] and confirms that the photon trap acts by total internal reflection, effectively serving as a waveguide to direct incident energy away from the removed regions and into the remaining absorber material.

6. Barrier infrared detectors

A new concept of strategy to achieve HOT detectors, so called barrier detector, has been proposed by Maimon and Wicks [35]. This type of detector can be implemented in different semiconductor materials. Its practical application has been demonstrated in InAs, InAsSb, and InAs/GaSb type-II superlattices (T2SLs) [36] and recently, also in HgCdTe ternary alloy [37].

Introducing of unipolar barriers in various designs based on T2SLs drastically changed the architecture of infrared detectors. The term “unipolar barrier” was coined to describe a barrier that can block one carrier type (electron or hole) but allows the un-impeded flow the other, as illustrated in Fig. 18. Unipolar barriers are used to impede the

flow of majority carrier dark current in photoconductors. The nBn detector is designed to reducing dark current (associated with SRH processes) and noise without impending photocurrent (signal). In particular, the barrier serves to reduce surface leakage current. The nBn band gap diagram is shown in Fig. 18. It somewhat resembles the typical p-n photodiode, except that the junction (space charge region) is replaced by an electron blocking unipolar barrier (B), and that the p-contact is replaced by an n-contact. It can be stated, that the nBn design is a hybrid between photoconductor and photodiode.

Figure 19 shows a typical Arrhenius plot of the dark current in a conventional diode and in an nBn detector. Because in nBn detector there is no depletion, the generation-recombination contribution to the dark current from the photon-absorbing layer is totally suppressed. The lower portion of Arrhenius plot for the standard photodiode has a slope that is roughly half that of the upper portion. The dashed line is an extension of the high temperature diffusion limited region to temperatures below T_0 . T_0 is defined as the crossover temperature at which the diffusion and generation-recombination currents are equal. In low-temperature region, a nBn

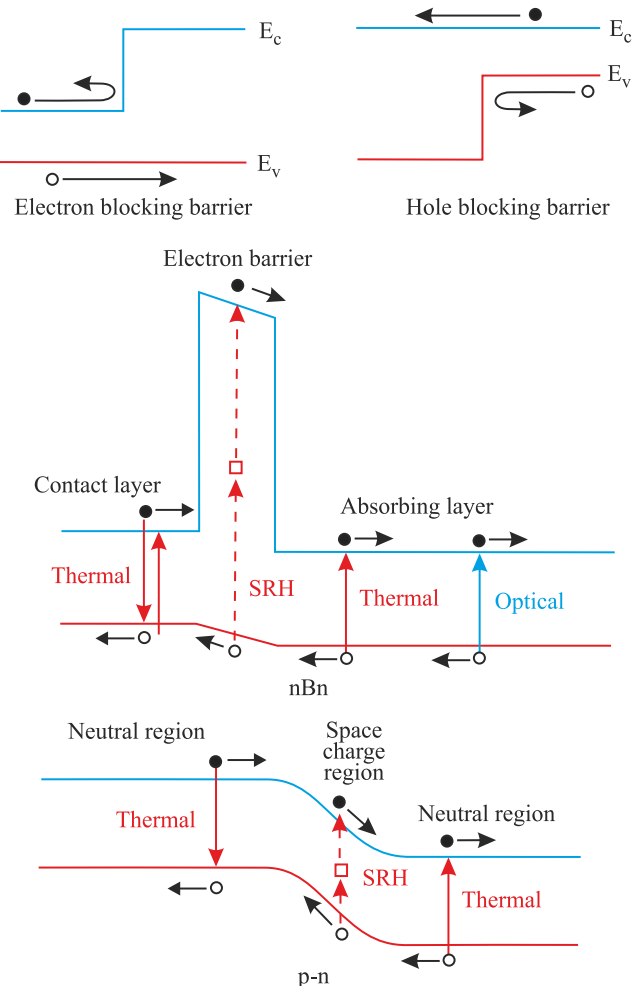


Fig. 18. Schematic illustrations of electron- and hole-blocking unipolar barriers, band gap diagram of nBn barrier detector and p-n photodiode.

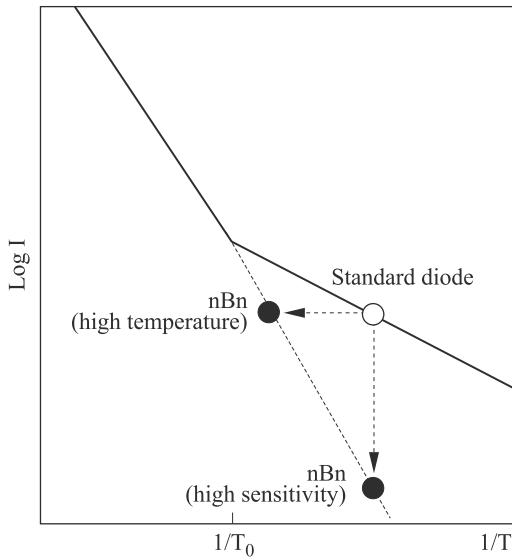


Fig. 19. Schematic Arrhenius plot of the dark current in a standard diode (solid line) and in an nBn device. Open circle shows the operating point of a standard diode while solid circles show operating points for the nBn device with improved sensitivity or higher operating temperature (adapted after Ref. 38).

detector offers two important advantages. First, it should exhibit a higher signal-to-noise ratio than a conventional diode operating at the same temperature. This is depicted by a vertical arrow in Fig. 19. Second, it will operate at a higher temperature than a conventional diode with the same dark current. This is depicted by a horizontal arrow in Fig. 19.

The operating principles of the nBn and related XBn detectors have been described in detail in the literature [35, 36, 38–40]. While the idea of nBn design was originated with bulk materials [35], its demonstration using T2SL based materials facilitates the experimental realization of the nBn concept with better control of band edge alignments [41]. Figure 20 shows an example of photovoltaic detector family: double heterostructure photodiode, pMp and pBn barrier detectors.

The pMp device consists of two p-doped superlattice active region and a thin M-structure with higher energy barrier. The band gap difference between superlattice and M-structure structures falls in the valence band, creating a valence band barrier for the majority holes in p-type semiconductor [42]. In the case of pBn structure, the p-n junction can be located at the interface between the heavily doped p-type material and the lower-doped barrier, or within the lower-barrier itself [43]. However, a key feature of the devices is a pair of complementary barriers, namely, an electron barrier and a hole barrier formed at different depths in the growth sequence. Such structure is known as complementary barrier infrared device (CBIRD) and was invented by Ting and others at JPL [44].

In the case of nBn detector, the n-type semiconductor on one side of the barrier constitutes a contact layer for biasing the device, while the n-type narrow-bandgap semiconductor on the other side of the barrier is a photon-absorbing layer

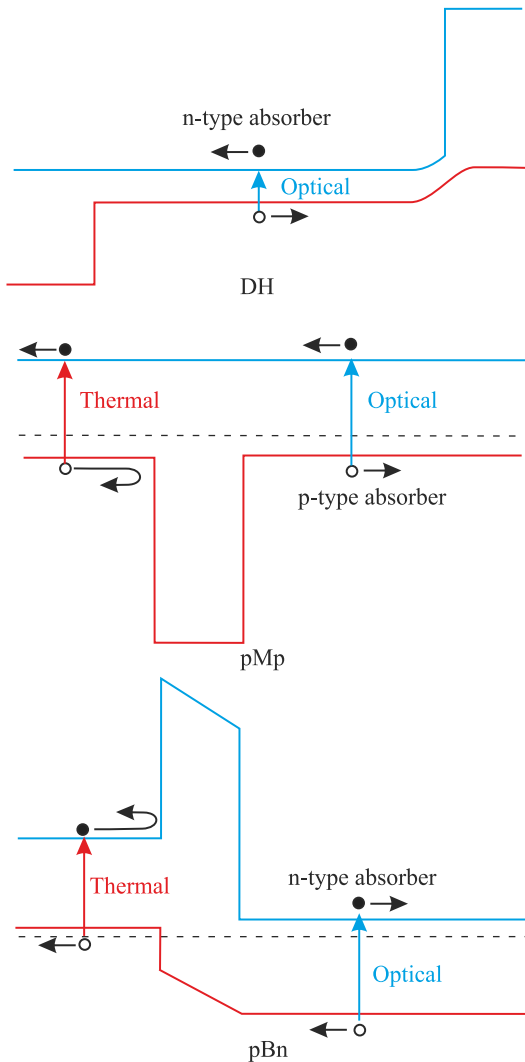


Fig. 20. Band gap diagrams of photovoltaic detectors: double heterostructure photodiode, pMp and pBn barrier detectors.

whose thickness should be comparable to the absorption length of light in the device, typically several microns.

Klipstein *et al.* and Weiss *et al.* have described [38, 45] the detailed growth procedure and device's characterization of $\text{InAs}_{1-x}\text{Sb}_x/\text{AlAs}_{1-y}\text{Sb}_y$ nBn MWIR detector. The n-type doping is usually reached by either Si or Te elements. The InAsSb structures were grown on either GaAs(100) or GaSb(100) substrates in a Veeco Gen200 MBE machine. The mismatched structures were grown on a 4- μm thick GaSb buffer layer, whereas the remaining structures were grown directly onto GaSb(100) substrates. The principal layers in the device structures were a thick n-type InAsSb absorption layer (1.5–3 μm), a thin n-type AlSbAs barrier layer (0.2–0.35 μm), and a thin (0.2–0.3 μm) n-type InAsSb contact layer. The bottom contact layer was highly doped. It must be stressed that in the real structure the n⁺ barrier for holes were not grown. Figure 21 shows an example of similar structure considered theoretically by Martyniuk and Rogalski [46].

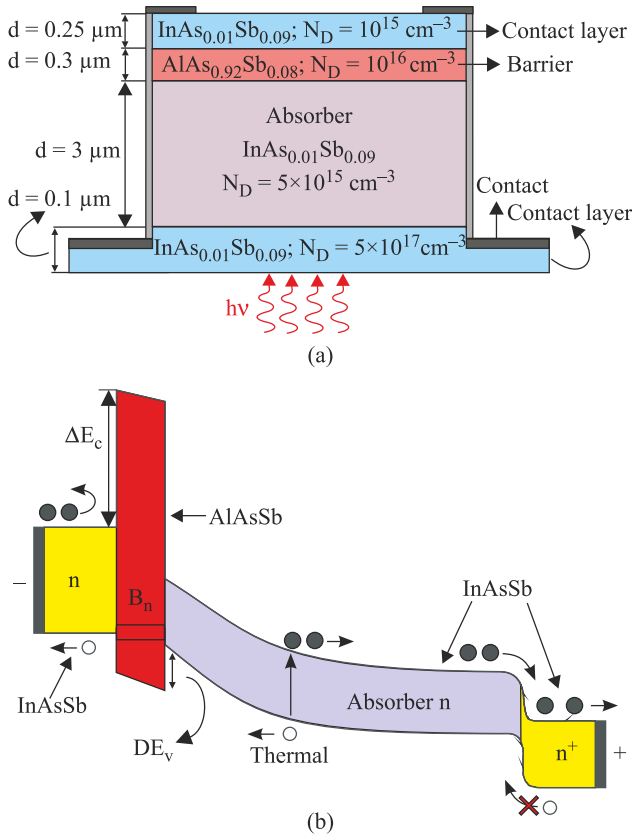


Fig. 21. InAsSb/AlAsSb nBn MWIR detector: the device structure (a) and the stimulated energy band diagram under reverse bias conditions.

Figure 22 shows the dependence of the room-temperature R_0A product vs. band gap energy of absorption layer (AL) in InAsSb/AlAsSb nBn detector and p-on-n InAsSb photodiode. The n-type and p-type constituent layers of the photodiode are assumed to be doped to the level of $N_D = 5 \times 10^{15} \text{ cm}^{-3}$ and $N_A = 5 \times 10^{17} \text{ cm}^{-3}$, respectively. The

RA product for InAsSb photodiode is calculated at reverse bias $V = -0.1 \text{ mV}$ while nBn counterpart is determined for selected voltages ($V = -250, -350$ and -500 mV). The RA product for nBn structure is higher in comparison to the p-on-n InAs_{1-x}Sb_x photodiode for the AL's $x > 0.15$, while for lower absorber's x-composition both RA products are comparable ($V = -500 \text{ mV}$). Once InAsSb's composition decreases, RA reaches its minimum and further increases is visible due to barrier creation in valance band. The InAsSb nBn performance is also compared to the HgCdTe "Rule 07" being the simple mean to compare IR detectors [47]. It is visible that InAsSb/AlAsSb nBn structures exhibit RA similar to the best R_0A HgCdTe photodiodes with the same AL energy bandgap.

In further estimations, the detectivity is considered at room temperature. It is assumed that the detectivity of p-on-n InAsSb photodiode is limited by thermal Johnson-Nyquist noise while nBn detector by thermal and electrical shot noise, respectively (nBn requires bias to operate). The optical shot noise is not included in simulations due to its negligible influence at room temperature conditions. Assuming the same AL's doping ($N_D = 5 \times 10^{15} \text{ cm}^{-3}$) the nBn structure reaches higher D^* only for $x > 0.20$. The p-on-n photodiodes exhibit better performance for $x < 0.15$. For room temperature operation, nBn structures with AL's compositions $x = 0.20$ could compete with p-on-n photodiode (limited by thermal noise) reaching $D^* \approx 5 \times 10^9 - 2 \times 10^{10} \text{ cmHz}^{1/2}/\text{W}$ for the same level of quantum efficiency (QE) equal 65 %. Lowering the Sb's composition in AL, the photodiode reaches nearly two times higher detectivities than nBn structure.

D'Souza *et al.* have demonstrated nBn device in the InAsSb/AlAsSb materials system grown by MBE on GaSb and GaAs substrates [34]. Similarly as previously, a large AlAsSb conduction band barrier suppresses the flow of majority carrier electrons, thus eliminating the electric field associated with a conventional p-n junction that results in high

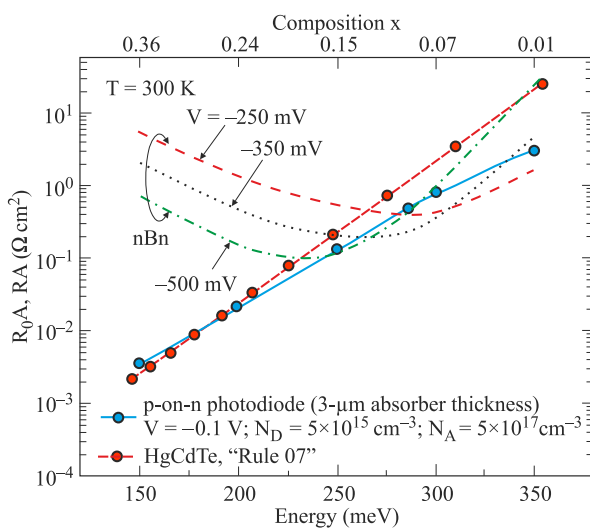


Fig. 22. R_0A and RA product of MWIR InAsSb/AlAsSb nBn detector and p-on-n InAsSb photodiode vs. InAsSb absorption layer band gap energy. R_0A is calculated in accordance with HgCdTe "Rule 07".

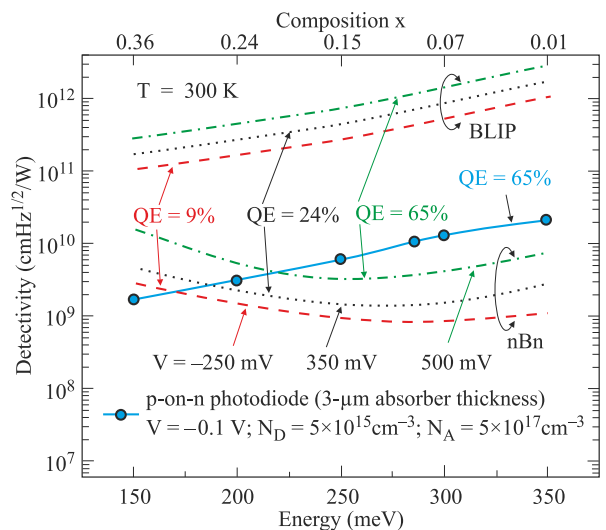


Fig. 23. Detectivity of MWIR InAsSb/AlAsSb nBn detector and p-on-n InAsSb photodiode vs. InAsSb absorption layer band gap energy.

dark currents associated with depletion region generation-recombination currents. A properly designed nBn structure facilitates diffusion-dominated detector performance determined by the bulk minority carrier (hole) lifetime. The pixels' array are defined very simply by etching through the contact layer up to the barrier. Figure 24(a) shows 5- μm cut-off nBn detector structure operated at 200 K with AlAsSb barrier and pyramid-shaped absorbers fabricated in the n-type InAsSb absorber. The dark current density in the pyramidal structured diodes is reduced by a factor of 2–3, which is consistent with the volume reduction due to pyramid formation. Based on optical simulation, the pyramidal structures minimize the reflection and provide > 90 % absorption over the entire 0.5 μm to 5.0 μm spectral range [see Fig. 24(b)].

Potential interest in III-V lattice-matched family set (InAs, GaSb, and AlSb) around 6.1 \AA results not only from unique inherited capabilities of the new artificial material with entirely different physical properties in comparison to the constituent layers, but also from the nearly zero band offsets leading to the desirable unipolar band alignments difficult to attain in HgCdTe. Even though, HgCdTe does not exhibit valance zero band offset, it is commonly known that bulk HgCdTe offers high quantum efficiency, therefore recently research groups have attempted to apply unipolar architecture to HgCdTe alloy (n type barrier) which offers technological advantages over p-n HgCdTe homojunction (simplifying the fabrication process) [37,48].

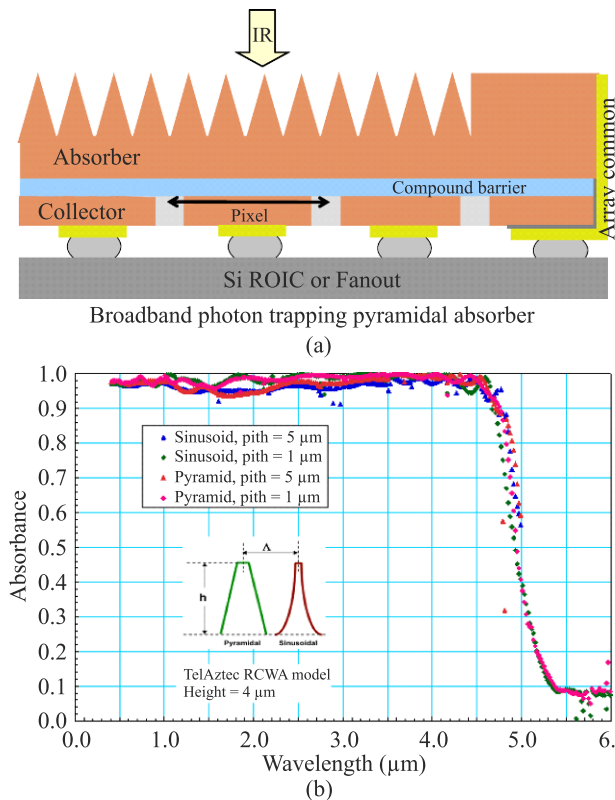


Fig. 24. Photon trapping nBn detector in the InAsSb/AlAsSb material system: (a) detector architecture with pyramid shaped absorber layer (after Ref. 34), (b) optical simulation of broadband detector response (after Ref. 33).

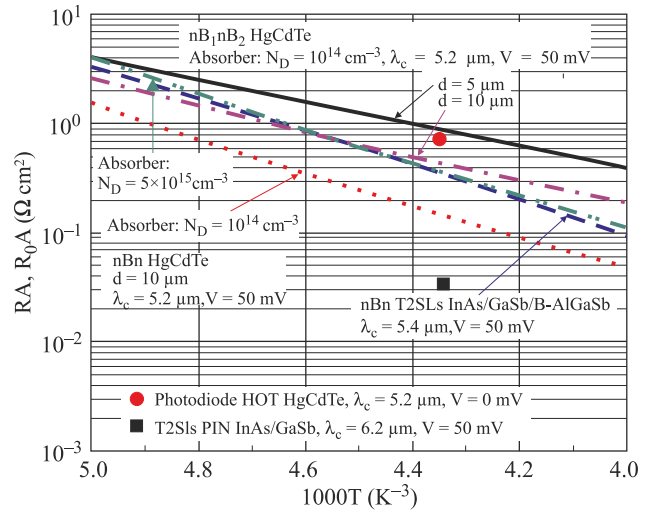


Fig. 25. Temperature dependence of the RA and R_0A products for MWIR complementary barrier HgCdTe detector, nBn HgCdTe detector, nBn InAs/GaSb/B-Al_{0.2}Ga_{0.8}Sb T2SL detector, HgCdTe HOT bulk diodes, and PIN InAs/GaSb T2SL diodes operating at near-room temperature ($T = 230$ K) (after Ref. 49). Experimental data for HgCdTe and PIN T2SL photodiodes are also shown.

Figure 25 compares the R_0A and RA products vs. temperature for MWIR complementary barrier HgCdTe detector (containing both electron and hole blocking barriers), unipolar nBn HgCdTe detector, InAs/GaSb/B-AlGaSb T2SL nBn detector ($\lambda_c = 5.4$ μm), InAs/GaSb PIN photodiode ($\lambda_c = 6.2$ μm), and finally HOT HgCdTe bulk photodiodes ($\lambda_c = 5.4$ μm) fabricated at the joint laboratory run by Institute of Applied Physics, Military University of Technology/Vigo System SA [49]. Theoretical estimation for the MWIR unipolar nBn HgCdTe/B-n type was conducted by Martyniuk and Rogalski in Ref. 50, whereas the performance of T2SLs nBn InAs/GaSb/B-Al-GaSb detector's performance was presented in Ref. 51 where an analytical approach was used to model the detectors's performance. PIN T2SLs photodiodes were analysed by Martyniuk *et al.* [52].

It is clearly seen that the performance of complementary barrier HgCdTe detector has reached a comparable level determined by the state of the art of HgCdTe bulk photodiodes and put itself in a superior position with reference to unipolar nBn HgCdTe/B-n type, T2SLs nBn, and PIN detectors. The particular significance of the incorporation of the extra barrier for minority carriers in complimentary barrier structures *vs.* single barrier (majority carriers' blocking) in unipolar nBn detectors is clearly evident by RA product increase from 0.1 to 0.5 Ωcm^2 for $T = 230$ K (for the same absorber).

7. Cascade infrared detectors

It is well known that in conventional photodiode the responsivity and diffusion length are closely coupled and an increase in the absorber thickness much beyond the diffusion length may not result in the desired improvement in signal to noise (S/N) ratio. This effect is particularly pro-

nounced at high temperatures, where diffusions lengths are typically reduced.

In a conventional photodiode only charge carriers that are photogenerated at a distance shorter than the diffusion length from junction can be collected. The absorption depth of LWIR radiation is longer than the diffusion length. Therefore, only a limited fraction of the photogenerated charge contributes to the quantum efficiency.

To avoid the limitation imposed by reduced diffusion length and effectively increase the absorption efficiency, novel detector designs, called cascade infrared detectors (CIDs) have been introduced in the last decade. CIDs contain multiple discrete absorbers, where each of them is shorter than the diffusion length. In this discrete CID absorber architecture, the individual absorbers are sandwiched between engineered electron and hole barriers to form a series of cascade stages. The photogenerated carriers travel only over one cascade stage before they recombine in the next stage, and every individual cascade stage can be significantly shorter than the diffusion length, while the total thickness of all the absorbers can be comparable or even longer than the diffusion length.

In this case, the S/N ratio and detectivity will continue to increase with multiple discrete absorbers resulting in improved device performance at elevated temperatures compared to a conventional p-n photodiode. In addition, flexibility to vary the number and thicknesses of discrete absorbers result in tailoring of CID design for optimized performance in meeting specific applications.

Different types of cascade IR detectors have been proposed between them two main classes are distinguished: so called intersubband (IS) unipolar quantum cascade IR detectors (QCIDs) and interband (IB) ambipolar CIDs.

Intersubband QCIDs are a fairly new development which has been evolving from the quantum cascade laser (QCL) research and which has been built for about 15 years [53–57]. A schematic comparison between the band structure of a photoconductive quantum well infrared photodetector (QWIP) and photovoltaic QCID is shown in Fig. 26. The QWIP structure is polarized in order to make the electrons circulate in the external circuit and to record the variation. The active detector region consists of identical QWs separated by thicker barriers. Electrons are excited either by photoemission (red arrows) or by thermionic emission (black arrows) from the quantum wells.

The QCIDs are usually created to be photovoltaic detectors. They consist of several identical periods made of one active doped well and some other coupled wells. The photoexcited electrons are transported from one active well to the next one by phonon emission through a cascade of levels. Figure 26(b) shows the conduction band of one period. Incident photon induces an electron to go from the ground state E_1 to the excited level E_2 which is next transferred to the right hand QWs through longitudinal optical phonon relaxations and finally to the fundamental subband of the next period. The detector period is repeated N times in order to increase the detectivity.

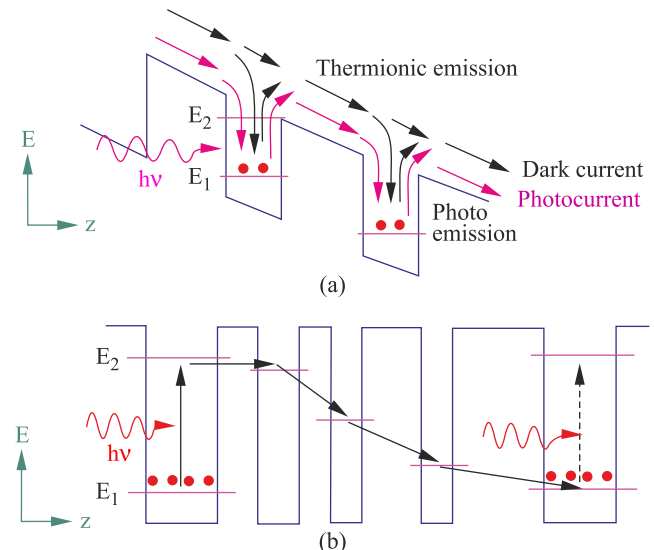


Fig. 26. Schematic conduction band diagram of a QWIP and QCID. In the QWIP, electron transport is accomplished by an external voltage bias whereas in QCID an internal potential ramp ensures the carrier transport (adapted after Ref. 56).

To describe the performance of IS quantum cascade IR detectors (QCIDs), it is convenient to use the formalism originally developed for QWIPs [58]. A theoretical model is presented e.g. in Refs. 53, 54, and 57.

Due to the photovoltaic character of IS QCID and assuming fundamental hypothesis that the diffusion is only due to electron LO-phonon interactions, a diode-like expression for the dark current density [53]

$$J_d(V) = J_s \left[\exp\left(\frac{qV}{NkT}\right) - 1 \right], \quad (10)$$

where $J_s = kT/qr_0A$ is the saturation current, r_0A is the resistance at zero bias times the detector area corresponding to one period of QCID, T is the detector temperature, V is the applied voltage, and N is the number of periods. Expression (10) represents the dark current produced by N identical diodes in series.

The doping dependence of dark current is contained in the r_0A expression

$$r_0A = \frac{kT}{q^2 \sum_{i \in A} \sum_{j \in B} G_{ij}}, \quad (11)$$

through the term G_{ij} which is the phonon interacted transition rate from the subband i of the cascade A to the subband j of the cascade B . The whole resistance of the detector, R_0 , is directly proportional to N

$$R_0A = Nr_0A. \quad (12)$$

Resistance of ICID can be much higher than for a conventional photodiode, since it is proportional to N and can be large for a structure with many barrier layers.

The detectivity of QCID, including Johnson noise and electrical shot noise components, is determined by [53]

$$D^* = \frac{\eta\lambda q}{hc} \left(\frac{4kT}{N r_0 A} + \frac{2qI_d}{N} \right)^{-1/2}, \quad (13)$$

so, the signal-to-noise ratio $S/N \propto \sqrt{N}$.

Promising technology of IS QCDs has been proven in a wavelength range from the near IR to the terahertz (THz) region as is presented in Fig. 27. At present well established semiconductor material systems and processing methods are available. At the beginning, QCDs have been demonstrated in the near-IR fabricated from InGaAs/AlAsSb, in the mid-IR using InGaAs/InAlAs, and in long-IR up to THz-region using GaAs/AlGaAs materials. These detectors have been cryogenically cooled [55,56].

Recently has been appeared that for near-room temperature detector operation more promising are bipolar devices based on type-II InAs/GaSb interband (IB) superlattice (SL) absorbers [59–63]. These interband cascade detectors combine the advantages of interband optical transitions with the excellent carrier transport properties of the interband cascade laser structures. Thermal generation rate at any specific temperature and cut-off wavelength in these devices is usually orders of magnitude smaller than for corresponding intersubband QCIDs. As a result their performance is better especially at room temperature (see Fig. 27). The operation idea of interband cascade photodetectors is similar to that shown in Fig. 6(b). Since design of interband cascade IR detectors (IB CIDs) is relatively complicated, with many interfaces and strained thin layers, their growth by MBE is challenging. In dependence on detector design, there are some key differences in the relaxation, the tunnelling region, and the contact layers. For example, below are shown and shortly described two types of detector designs.

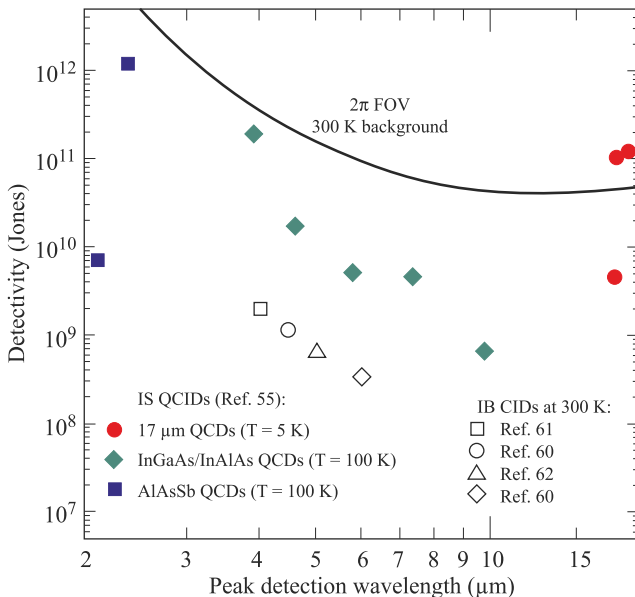


Fig. 27. Detectivity as function of wavelength for different types of CIDs.

Tian *et al.* have proposed a structure shown schematically in Fig. 28 [61]. The detector consists of a $0.5 \mu\text{m}$ p-type GaSb buffer layer, then a 7-stage interband cascade structure using a finite InAs/GaSb type-II SL (T2SL) as an absorber, and finally a 45-nm-thick n-type InAs top contact layer. Each cascade stage is composed of a thin InAs/GaSb (7 ML/9 ML) T2SL absorber, where GaSb is sandwiched between the electron relaxation and the interband-tunnelling regions served also as hole and electron barriers, respectively. The barrier acts as a means for suppressing leakage current. The electron-relaxation region is designed to facilitate the extraction of photogenerated carriers from the conduction miniband of the absorber and transport them ideally (with little or no resistance) to the valence band of the absorber in the next stage. The energy levels of coupled InAs/AlSb multi-quantum wells (QWs) form a staircase, with energy separations comparable to the LO-phonon energy. The uppermost energy level of the relaxation region staircase is close to the conduction miniband in the InAs/GaSb SL, and the bottom energy-level is positioned below the valence-band edge of the adjacent GaSb layer, allowing the interband tunnelling of extracted carriers to the next stage. Figure 28(b) shows two channels through which an electron can tunnel through to the next stage: interband tunnelling through the type-II broken gap, and intraband tunnelling across or thermionic emission over the electron barrier. The enhanced electron barriers suppress intraband-tunnelling current between stages and p-type type-II InAs/GaSb superlattice absorbers.

Next figure (Fig. 29) presents the Johnson-noise limited detectivity spectra at various temperatures, extracted from the measured responsivity spectra and R_0A product for one of the above detector structure. The dark current density at

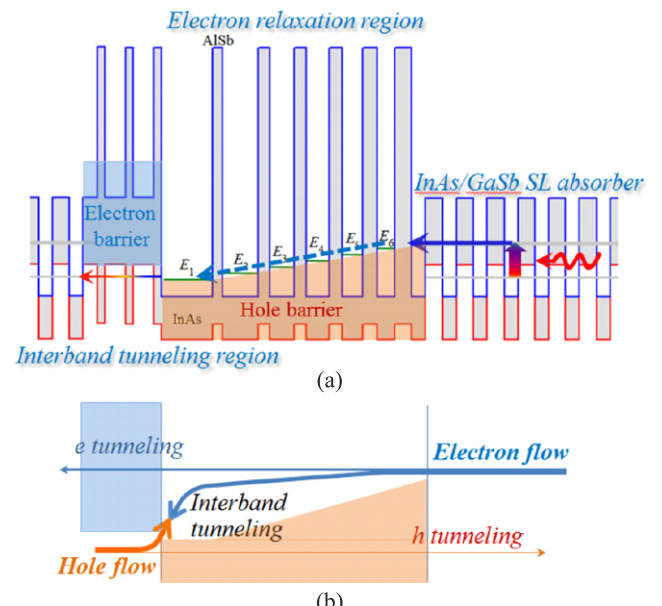


Fig. 28. Schematic illustration of the interband cascade type-II InAs/GaSb superlattice photodetector: (a) photocarrier dynamics, and (b) dark current dynamics (after Ref. 61).

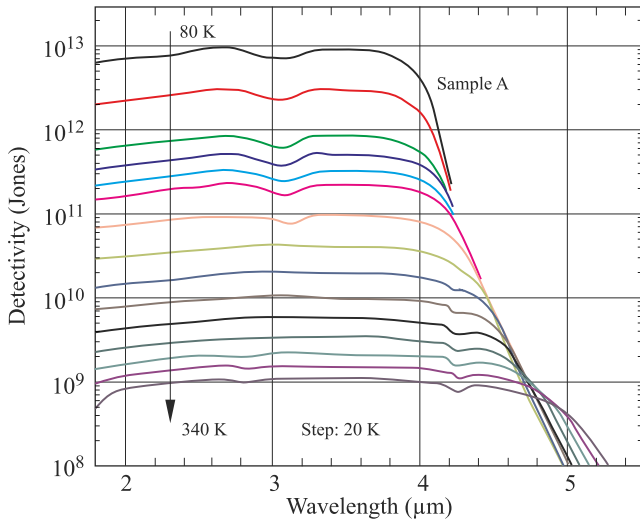


Fig. 29. Johnson-noise limited detectivity spectra of interband cascade type-II InAs/GaSb superlattice photodetector at various temperatures (after Ref. 61).

-50 mV is 2.8×10^{-2} A/cm 2 at 300 K, and the extracted R_0A is $1.9 \Omega \text{cm}^2$, corresponding to a Johnson-noise limited D^* of 2×10^9 Jones at 4.5 μm .

Modification of the MWIR detector structure has been proposed by Gautam *et al.* [62]. A cartoon representation of one stage of the cascade detector is shown in Fig. 30(a) with absorber region (1), interband tunnelling region (2) and the transport region (3). Due to built-in electric field, photo-generated electron-hole pairs in the absorber region (1) move in opposite directions: electrons to the right while the holes – to the left. The separation between the quantized energy level in the GaSb QW of region (2) and the valance band in region (1) is designed to be equal to the LO-phonon

energy in AlSb (to make the tunnelling of holes a photon-assisted process). The hole and electron barriers represented by the relaxation region (3) and the interband tunnelling region (2) also act as hole and electron barriers and block the flow of dark carriers from one cascade stage into the other.

The heterostructure schematic of the QCD structure is illustrated in Fig. 30(b). It consists a bottom n⁺-type InAs/AlSb T2SL contact layer followed by seven cascade stages, which precede a 2-nm thick AlSb tunnelling barrier, and then the top contact layer. The absorber, non-intentionally doped region, is made from 9ML InAs/9ML GaSb T2SL.

In the present design, the total thickness of the absorber is about 1 μm , and the absorption quantum efficiency should increase by increasing the number of stages. However the conversion quantum efficiency is lower than that of the absorption quantum efficiency by a factor of N .

The spectral responsivity of MWIR T2SL cascade detector with 7- μm cut-off wavelength has been observed up to 420 K at bias voltage of 0.5 V (see Fig. 31). At room temperature and at wavelength $\approx 4 \mu\text{m}$, the Johnson noise limited detectivity is 8.9×10^8 Jones. The performance of the device can further be improved by optimizing the doping in the absorber and barrier regions.

The transport of photoexcited carriers is very fast and occurs over a very short distance (≈ 50 –200 nm depending on wavelength) in each cascade stage, and is much shorter than a typical diffusion length. In such condition, the lateral diffusion transport may not be significant over such a short distance and, thus the deeply etched mesa structures for confining photoexcited carriers may not be necessary in QCDs in contrast to conventional photodiodes. Moreover, significant wave function overlap of energy states in the multiple QW region (relaxation region) causes that the intersubband

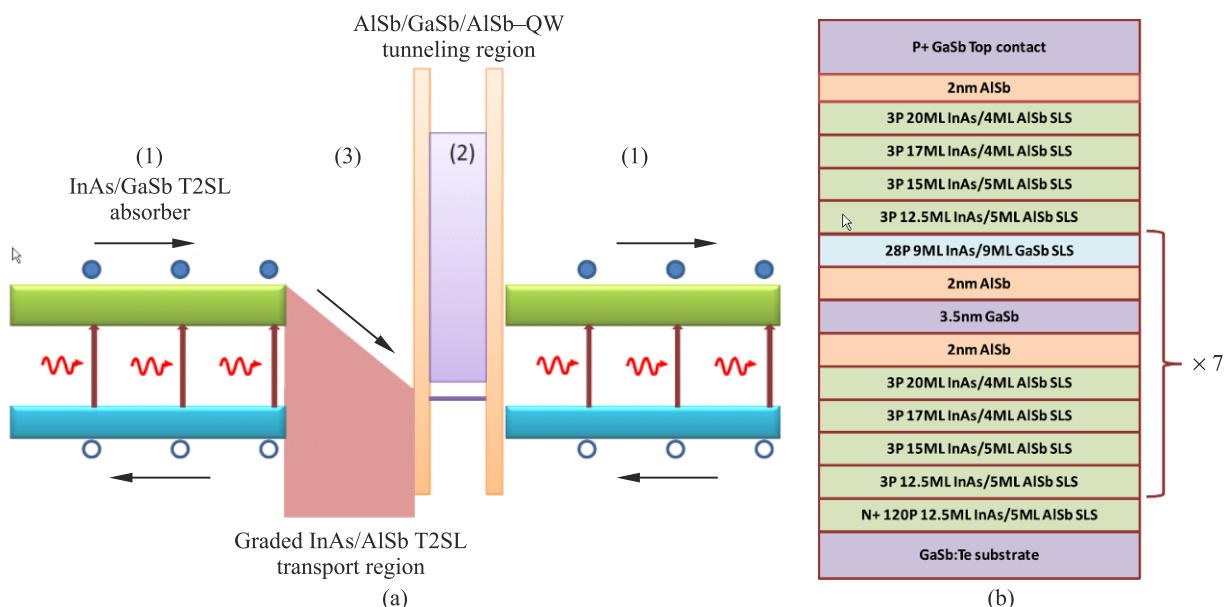


Fig. 30. MWIR T2SL interband cascade detector: (a) a cartoon representation of one stage and (b) schematic of the detector structure (after Refs. 62,63).

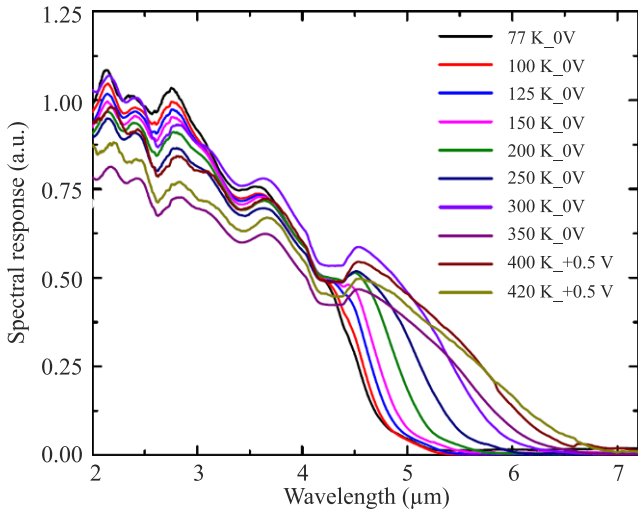


Fig. 31. Measured photocurrent signal of MWIR T2SL interband cascade detector as a function of temperature (after Ref. 62).

relaxation time (e.g., optical-phonon scattering time ≈ 1 ps) is much shorter than the interband recombination time (≈ 1 ns, or ≈ 0.1 ns at high temperatures with more Auger recombination). Consequently, the photoexcited electrons in the active region are transferred to the bottom of the energy ladder with a very high efficiency. This mechanism enables the quick and efficient removal of carriers after photoexcitation.

At present HgCdTe is the most widely used variable gap semiconductor for IR photodetectors also for uncooled operation. Especially the resistance of HgCdTe photodiodes operated in a long wavelength IR region is very low due to a high thermal resistance. For example, small size uncooled 10.6- μm photodiodes ($50 \times 50 \mu\text{m}^2$) exhibit less than 1Ω zero bias junction resistances which are well below the series resistance of a diode. As a result, the performance of conventional devices is very poor, so they are not usable for practical applications.

Figure 32 compares the R_0A product of HgCdTe photodiodes with room-temperature experimental data for interband CIDs fabricated with type-II InAs/GaSb SL absorbers. It is clearly shown that at present stage of CID technology, their experimentally measured R_0A values at room temperature are higher than those for the state-of-the-art HgCdTe photodiodes. However, their quantum efficiency is low, typically below 10%.

It can be predicted that with a better understanding of the quantum cascade device physics and other aspects related to their design and material properties will enable high performance HOT detectors. In addition, the discrete architecture of QCD provides a great deal of flexibility for manipulating carrier transport to achieve high-speed operation which determines the maximal bandwidth. The possibility of having them monolithically integrated with active components, for instance lasers, offers entirely new avenues for telecommunication systems based on quantum devices.

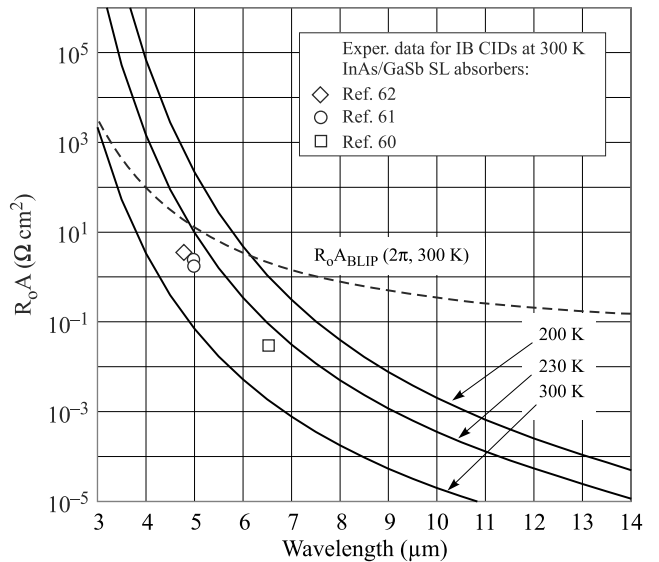


Fig. 32. R_0A product of HgCdTe photodiodes (solid lines) in comparison with room-temperature experimental data for IB CIDs with type-II InAs/GaSb SL absorbers.

8. Conclusions

Photodetectors are based on photogeneration of electrons and holes in a semiconductor material, followed by subsequent collection of the created charge. They have important advantages compared to the thermal detectors. Since no thermal processes are involved in a detection process, photodetectors exhibit very fast response. In contrast to thermal detectors, the performance of photodetectors exponentially decreases with an increasing cut-off wavelength and temperature of operation. As a result, the uncooled LWIR devices are typically characterized by poor performance.

Uncooled LWIR photodetectors are less developed compared to the competition thermal detectors, however. Their availability is limited to a single element and small arrays. The main problem is their low resistance that prevents use of well-developed CMOS readout circuits. This can be solved with a development of integrated microoptics, multiple heterojunctions, Auger suppressed devices, and new generation of cascade detectors.

Currently, the only commercially available fast room temperature detectors in the LWIR range are HgCdTe photodetectors. New materials, such as InAsSb and type-II superlattices have demonstrated the capability to provide uncooled performance equivalent to thermal detectors with cut-off frequencies' orders of higher magnitude. Being grown on the GaAs substrates, these III-V material systems are promising for the future integration with Si technology. However, hitherto, no practical devices based on this technology are available.

At present, uncooled thermal detectors are clearly the winner in the race for uncooled thermal imaging. At the same time, further improvement in thermal and spatial resolution of thermal imagers based on FPAs with thermal

detectors remains a substantial challenge. For thermal detectors it will require a clever design to include an IR absorber in a very low mass pixel structure. Future development may involve devices based on new principles of the operation.

In the case of infrared HOT photodetectors several new strategies have been used in the last decade including barrier detectors, photon trapping detectors, intersubband and interband cascade detectors. Especially, more promising are interband cascade devices based on type-II InAs/GaSb interband superlattice absorbers. At present stage of technology, their experimentally measured R_0A values at room temperature are higher than those predicted for HgCdTe photodiodes. A better understanding of device physics and improving their design can enable achieving of high performance HOT detectors.

References

- J. Piotrowski and A. Rogalski, "Uncooled long wavelength infrared photon detectors," *Infrared Physics & Technol.* **46**, 115–131 (2004).
- J. Piotrowski and A. Rogalski, *High-Operating Temperature Infrared Photodetectors*, SPIE Press, Bellingham, 2007.
- J. Piotrowski and A. Piotrowski, "Room temperature IR photodetectors," in *Mercury Cadmium Telluride. Growth, Properties and Applications*, edited by P. Capper and J. Garland, pp. 513–537, Wiley, West Sussex, 2011.
- A. Rogalski, *Infrared Detectors*, CRC Press, Boca Raton, 2011.
- J. Piotrowski and A. Rogalski, "Photoelectromagnetic, magnetoconcentration and Dember infrared detectors" in *Narrow-Gap II-VI Compounds and Electromagnetic Applications*, pp. 506–525, edited by P. Capper, Chapman & Hall, London, 1997.
- C.T. Elliott and N.T. Gordon, "Infrared detectors", in *Handbook on Semiconductors*, Vol. 4, pp. 841–936, edited by C. Hilszum, North-Holland, Amsterdam (1993).
- C.T. Elliott, "Non-equilibrium mode of operation of narrow-gap semiconductor devices", *Semicond. Sci. Technol.* **5**, S30–S37 (1990).
- T. Elliott, "New infrared and other applications of narrow gap semiconductors," *Proc. SPIE* **3436**, 763–775 (1998).
- Z. Djuric and J. Piotrowski, "Infrared photodetector with electromagnetic carrier depletion," *Opt. Eng.* **31**, 1955–1960 (1992).
- J. Piotrowski, W. Gawron, and Z. Djuric, "New generation of near-room-temperature photodetectors", *Opt. Eng.* **33**, 1413–1421 (1994).
- C.T. Elliott, "Photoconductive and non-equilibrium devices in HgCdTe and related alloys," in *Infrared Detectors and Emitters: Materials and Devices*, pp. 279–312, edited by P. Capper and C.T. Elliott, Kluwer Academic Publishers, Boston, 2001.
- J. Piotrowski and A. Rogalski, "Comment on ‘Temperature limits on infrared detectivities of InAs/In_xGa_{1-x}Sb superlattices and bulk Hg_{1-x}Cd_xTe’ [J. Appl. Phys. **74**, 4774 (1993)]", *J. Appl. Phys.* **80**, 2542–2544 (1996).
- J. Piotrowski and W. Gawron. "Ultimate performance of infrared photodetectors and figure of merit of detector material", *Infrared Physics and Technol.* **38**, 63–68 (1997).
- <http://www.vigo.com.pl/>
- <http://www.vigo.com.pl/index.php/en/content/download/2411/10089/file/catalogue%20512.pdf>
- A. Piotrowski, P. Madejczyk, W. Gawron, K. Kłos, J. Pawłuczyk, J. Rutkowski, J. Piotrowski, A. Rogalski, "Progress in MOCVD growth of HgCdTe heterostructures for uncooled infrared photodetectors", *Infrared Physics & Technol.* **49**, 173–182 (2007).
- P. Madejczyk, W. Gawron, A. Piotrowski, K. Kłos, J. Rutkowski, and A. Rogalski, "Improvement in performance of high-operating temperature HgCdTe photodiodes", *Infrared Physics & Technol.* **54**, 310–315 (2011).
- J.D. Kim and M. Razeghi, "Investigation of InAsSb infrared photodetectors for near-room temperature operatio,", *Opto-Electron. Rev.* **6**, 217–230 (1998).
- H. Mohseni, J. Wojkowski, M. Razeghi, G. Brown, and W. Mitchel, "Uncooled atmospheric window InAs-GaSb type-II infrared detectors grown on GaAs substrates for the 8–12 μm ", *IEEE J. Quantum Electron.* **35**, 1041–1044 (1999).
- P.W. Kruse, "Indium antimonide photoelectromagnetic infrared detector," *J. Appl. Phys.* **30**, 770–778 (1959).
- E. Michel and M. Razeghi, "Recent advances in Sb-based materials for uncooled infrared photodetectors", *Opt.-Electr. Rev.* **6**, 11–23 (1998).
- E.G. Camargo, K. Ueno, T. Morishita, M. Sato, H. Endo, M. Kurihara, K. Ishibashi, and M. Kuze, "High-sensitivity temperature measurement with miniaturized InSb mid-IR sensor", *IEEE Sensors J.* **7**, 1335–1339 (2007).
- M. Kuze, T. Morishita, E.G. Camargo, K. Ueno, A. Yokoyama, M. Sato, H. Endo, Y. Yanagita, S. Tokuto, and H. Goto, "Development of uncooled miniaturized InSb Photo voltaic infrared sensors for temperature measurements", *J. Crystal Growth* **311**, 1889–1892 (2009).
- A. Rogalski, "InAs_{1-x}Sb_x infrared detectors," *Prog. Quantum Electron.* **13**, 191–231 (1989).
- P. Knowles, L. Hipwood, N. Shorrocks, I. M. Baker, L. Pillans, P. Abbott, R. Ash, and J. Harji, "Status of IR detectors for high operating temperature produced by MOVPE growth of MCT on GaAs substrates", *Proc. SPIE* **8541**, 854108 (2012). doi:10.1117/12.971431.
- L. Pillans, R.M. Ash, L. Hipwood, and P. Knowles, "MWIR mercury cadmium telluride detectors for high operating temperatures", *Proc. SPIE* **8353**, 83532W (2012).
- R. DeWames and J. Pellegrino, "Electrical characteristics of MOVPE grown MWIR N⁺p(As) HgCdTe hetero-structure photodiodes build on GaAs substrates", *Proc. SPIE* **8353**, 83532P (2012).
- J.G.A. Wehner, E.P.G. Smith, G.M. Venzor, K.D. Smith, A.M. Ramirez, B.P. Kolasa, K.R. Olsson, and M.F. Vilela, "HgCdTe photon trapping structure for broadband mid-wavelength infrared absorption", *J. Electron. Mater.* **40**, 1840–1846 (2011).
- K.D. Smith, J.G.A. Wehner, R.W. Graham, J.E. Randolph, A.M. Ramirez, G.M. Venzor, K. Olsson, M.F. Vilela, and E.P.G. Smith, "High operating temperature mid-wavelength infrared HgCdTe photon trapping focal plane arrays", *Proc. SPIE* **8353**, 83532R (2012).
- D.A.G. Bruggeman, "Berechnung verschiedener physikalischer Konstanten von heterogenen Substanzen", *Ann. Phys. (Leipzig)* **24**, 636–679 (1935).
- K.T. Posani, V. Tripathi, S. Annamalai, S. Krishna, R. Perahia, O. Crisafulli, and O. Painter, "Quantum dot photonic crystal detectors", *Proc. SPIE* **6129**, 612906–1–8 (2006).

32. S. Krishna, K.T. Posani, V. Tripathi, S. Annamalai, R. Perahia, O. Crisafulli, and O. Painter, "Quantum dot infrared sensors with photonic crystal cavity", *Proc. Laser & Electro-optical Society*, Vol. 1, pp. 909–910, 2005.
33. N.K. Dhar and R. Dat, "Advanced imaging research and development at DARPA", *Proc. SPIE* **8353**, 835302 (2012).
34. A.I. D'Souza, E. Robinson, A.C. Ionescu, D. Okerlund, T.J. de Lyon, R.D. Rajavel, H. Sharifi, D. Yap, N. Dhar, P.S. Wijewarnasuriya, and C. Grein, "MWIR InAs_{1-x}Sb_x nCBn detectors data and analysis", *Proc. SPIE* **8353**, 835333 (2012).
35. S. Maimon and G.W. Wicks, "nBn detector, an infrared detector with reduced dark current and higher operating temperature", *Appl. Phys. Lett.* **89**, 151109 (2006).
36. D.Z.-Y. Ting, A. Soibel, L. Höglund, J. Nguyen, C.J. Hill, A. Khoshakhlagh, and S.D. Gunapala, "Type-II superlattice infrared detectors", in *Semiconductors and Semimetals*, Vol. 84, pp. 1–57, edited by S.D. Gunapala, D.R. Rhiger, and C. Jagadish, Elsevier, Amsterdam, 2011.
37. A.M. Itsuno, J.D. Philips, and S. Velicu, "Design and modeling of HgCdTe nBn detectors", *J. Elect. Mater.* **40**, 1624–1629 (2011).
38. P. Klipstein, "XBn' barrier photodetectors for high sensitivity and high operating temperature infrared sensors", *Proc. SPIE* **6940**, 69402U-1–11 (2008).
39. D.Z. Ting, C.J. Hill, A. Soibel, J. Nguyen, S.A. Keo, M.C. Lee, J.M. Mumolo, J.K. Liu, and S.D. Gunapala, "Antimonide-based barrier infrared detectors", *Proc. SPIE* **7660**, 76601R-1–12 (2010).
40. P. Klipstein, O. Klin, S. Grossman, N. Snapi, I. Lukomsky, D. Aronov, M. Yassen, A. Glzman, T. Fishman, E. Berkowicz, O. Magen, I. Shtrichman, and E. Weiss, "Bn barrier photodetectors based on InAsSb with high operating temperatures", *Opt. Eng.* **50**, 061002-1–10 (2011).
41. J.B. Rodriguez, E. Plis, G. Bishop, Y.D. Sharma, H. Kim, L.R. Dawson, and S. Krishna, "nBn structure based on InAs/GaSb type-II strained layer superlattices", *Appl. Phys. Lett.* **91**, 043514-1–2 (2007).
42. B.-M. Nguyen, S. Bogdanov, S.A. Pour, and M. Razeghi, "Minority electron unipolar photodetectors based on type II InAs/GaSb/AlSb superlattices for very long wavelength infrared detection", *Appl. Phys. Lett.* **95**, 183502-1–3 (2009).
43. A.D. Hood, A.J. Evans, A. Ikhlassi, D.L. Lee, and W.E. Tennant, "LWIR strained-layer superlattice materials and devices at Teledyne Imaging Sensors", *J. Electron. Mater.* **39**, 1001–1006 (2010).
44. D.Z.-Y. Ting, C.J. Hill, A. Soibel, S.A. Keo, J.M. Mumolo, J. Nguyen, and S.D. Gunapala, "A high-performance long wavelength superlattice complementary barrier infrared detector", *Appl. Phys. Lett.* **95**, 023508-1–3 (2009).
45. E. Weiss, O. Klin, S. Grossmann, N. Snapi, I. Lukomsky, D. Aronov, M. Yassen, E. Berkowicz, A. Glzman, P. Klipstein, A. Fraenkel, and I. Shtrichman, "InAsSb-based XBnn bariodes grown by molecular beam epitaxy on GaAs", *J. Crystal Growth* **339**, 31–35 (2012).
46. P. Martyniuk and A. Rogalski, "Modelling of InAsSb/AlAsSb nBn HOT detector's performance limit", to be published.
47. W.E. Tennant, D. Lee, M. Zandian, E. PiQuette, and M. Carmody, "MBE HgCdTe technology: A very general solution to IR detection, described by "Rule07", a very convenient heuristic", *J. Electron. Mater.* **37**, 1406–1410 (2008).
48. S. Velicu, J. Zhao, M. Morley, A.M. Itsuno, and J.D. Philips, "Theoretical and experimental investigation of MWIR HgCdTe nBn detectors", *Proc. SPIE* **8268**, 82682X (2012).
49. P. Martyniuk and A. Rogalski, "Modelling of MWIR HgCdTe complementary barrier HOT detector", *Solid-State Electron.* **80**, 96–104 (2013).
50. P. Martyniuk and A. Rogalski, "Theoretical modelling of MWIR thermoelectrically cooled nBn HgCdTe detector", to be published in *Bull. Pol. Ac.: Tech.*
51. P. Martyniuk, J. Wróbel, E. Plis, P. Madejczyk, A. Kowalewski, W. Gawron, S. Krishna, and A. Rogalski, "Performance modeling of MWIR InAs/GaSb/B-Al_{0.2}Ga_{0.8}Sb type-II superlattice nBn detector", *Semicond. Sci. Technol.* **27**, 055002 (2012).
52. P. Martyniuk, J. Wróbel, E. Plis, P. Madejczyk, W. Gawron, A. Kowalewski, S. Krishna, and A. Rogalski, "Modelling of mid wavelength infrared InAs/GaSb type II superlattice detectors", *Opt. Eng.* **52**, 061307-1–12 (2013).
53. A. Gomez, M. Carras, A. Nedelcu, E. Costard, X. Marcadet, V. Berger, "Advantages of quantum cascade detectors", *Proc. SPIE* **6900**, 69000J-1–14 (2008).
54. F.R. Giorgetta, E. Baumann, M. Graf, Q. Yang, C. Manz, K. Köhler, H.E. Beere, D.A. Ritchie, E. Linfield, A.G. Davies, Y. Fedoryshyn, H. Jäckel, M. Fischer, J. Faist, and D. Hofstetter, "Quantum cascade detectors", *IEEE J. Quantum Electron.* **45**, 1039–1052 (2009).
55. D. Hofstetter, F.R. Giorgetta, E. Baumann, Q. Yang, C. Manz, and K. Köhler, "Mid-infrared quantum cascade detectors for applications in spectroscopy and pyrometry", *Appl. Phys. B* **100**, 313–320 (2010).
56. A. Buffaz, M. Carras, L. Doyennette, A. Nedelcu, P. Bois, and V. Berger, "State of the art of quantum cascade photodetectors", *Proc. SPIE* **7660**, 76603Q-1–10 (2010).
57. A. Buffaz, A. Gomez, M. Carras, L. Doyennette, and V. Berger, "Role of subband occupancy on electronic transport in quantum cascade detectors", *Phys. Rev. B* **81**, 075304-1–8 (2010).
58. H. Schneider and H.C. Liu, *Quantum Well Infrared Photodetectors*, Springer, Berlin, 2007.
59. J.V. Li, R.Q. Yang, C.J. Hill, and S.L. Chung, "Interband cascade detectors with room temperature photovoltaic operation", *Appl. Phys. Lett.* **86**, 101102-1–3 (2005).
60. R.Q. Yang, Z. Tian, Z. Cai, J.F. Klem, M.B. Johnson, and H.C. Liu, "Interband-cascade infrared photodetectors with superlattice absorbers", *J. Appl. Phys.* **107**, 054514-1–6 (2010).
61. Z. Tian, R.T. Hinkey, R.Q. Yang, D. Lubyshev, Y. Qiu, J.M. Fastenau, W.K. Liu, and M.B. Johnson, "Interband cascade infrared photodetectors with enhanced electron barriers and p-type superlattice absorbers", *J. Appl. Phys.* **111**, 024510-1–6 (2012).
62. N. Gautam, S. Myers, A.V. Barve, B. Klein, E.P. Smith, D.R. Rhiger, L.R. Dawson, and S. Krishna, "High operating temperature interband cascade midwave infrared detector based on type-II InAs/GaSb strained layer superlattice", *Appl. Phys. Lett.* **101**, 021106-1–4 (2012).
63. N. Gautam, "Unipolar barrier strained layer superlattice infrared photodiodes: physics and barrier engineering", *Dissertation*, The University of New Mexico, Albuquerque, 2012.